Inorganic polyphosphate interacts with nucleolar and glycosomal proteins in trypanosomatids

Raquel S. Negreiros,[1,#] Noelia Lander,[1,2]
Guozhong Huang,[1] Ciro D. Cordeiro,[1,2]
Stephanie A. Smith,[3] James H. Morrissey[3] and
Roberto Docampo (iD) [1,2*]
[1]Center for Tropical and Emerging Global
Diseases, University of Georgia, Athens, GA 30602,
USA.
[2]Department of Cellular Biology, University of Georgia,
Athens, GA 30602, USA.
[3]Department of Biological Chemistry, University of
Michigan Medical School, Ann Arbor, MI 48109, USA.

Summary

Inorganic polyphosphate (polyP) is a polymer of three to hundreds of phosphate units bound by high-energy phosphoanhydride bonds and present from bacteria to humans. Most polyP in trypanosomatids is concentrated in acidocalcisomes, acidic calcium stores that possess a number of pumps, exchangers, and channels, and are important for their survival. In this work, using polyP as bait we identified > 25 putative protein targets in cell lysates of both *Trypanosoma cruzi* and *Trypanosoma brucei*. Gene ontology analysis of the binding partners found a significant over-representation of nucleolar and glycosomal proteins. Using the polyphosphate-binding domain (PPBD) of *Escherichia coli* exopolyphosphatase (PPX), we localized long-chain polyP to the nucleoli and glycosomes of trypanosomes. A competitive assay based on the pre-incubation of PPBD with exogenous polyP and subsequent immunofluorescence assay of procyclic forms (PCF) of *T. brucei* showed polyP concentration-dependent and chain length-dependent decrease in the fluorescence signal. Subcellular fractionation experiments confirmed the presence of polyP in glycosomes of *T. brucei* PCF. Targeting of yeast PPX to the glycosomes of PCF resulted in polyP hydrolysis, alteration in their glycolytic flux and increase in their susceptibility to oxidative stress.

Introduction

African trypanosomiasis, caused by the *Trypanosoma brucei* group of parasites, and Chagas disease, caused by *Trypanosoma cruzi,* are neglected tropical diseases that affect millions of people, causing thousands of deaths and affecting the ability of people to earn a living. Vaccines are not available and drug treatments have serious side effects or are not completely effective. The study of metabolic pathways in these parasites that may be essential for their survival could provide information on potential new targets that could be exploited for development of new therapeutic approaches.

Trypanosomatids are characterized by the compartmentation of the first six or seven enzymes of the glycolytic pathway in a peroxisome-like organelle, which for this reason was named the glycosome (Opperdoes and Borst, 1977), and by their high content of inorganic polyphosphate (polyP) that accumulates in acidocalcisomes, acidic calcium stores also rich in other organic and inorganic cations (Docampo and Huang, 2016). PolyP is a polymer of three to hundreds of high-energy phospho-anhydride-bonded orthophosphate units, and is universally conserved (Kornberg, 1995).

Although polyP accumulates in acidocalcisomes and acidocalcisome-like vacuoles (Docampo *et al.*, 2005) of eukaryotes, it has also been found in most cellular compartments including mitochondria (Lynn and Brown, 1963), cytosol (Kulaev and Kulakovskaya, 2000), endoplasmic reticulum (Vorisek *et al.*, 1982), nucleus (Griffin *et al.*, 1965), nucleolus (Jimenez-Nunez *et al.*, 2012), plasma membrane (Kumble and Kornberg, 1995) and lysosomes (Pisoni and Lindley, 1992). Rat liver nuclei and plasma membranes have several times the polyP concentration found in cytosol, mitochondria, and microsomes (Kumble and Kornberg, 1995). Early work proposed that polyP is covalently bound to non-histone nuclear proteins (Offenbacher and Kline, 1984), a concept that was revived by the demonstration in yeast that nucleolar proteins Nsr1

and Top1 can be polyphosphorylated in lysine residues (Azevedo *et al.*, 2015). Interestingly, recent work reported the polyphosphorylation of 15 target proteins in yeast, including a conserved network of proteins of nucleolar localization involved in ribosome biogenesis (Bentley-DeSousa *et al.*, 2018). Nucleolar polyP was also found in myeloma cells and proposed to regulate RNA polymerase I activity (Jimenez-Nunez *et al.*, 2012).

Several studies have shown that bacteria or unicellular eukaryotes lacking polyP are more sensitive to different stress conditions, including heat shock, osmotic stress, starvation and reactive oxygen species, among others (Rao *et al.*, 2009; Moreno and Docampo, 2013). The reason for this was never clearly understood until recent studies shed light on one possible mechanism behind this phenomenon (Kampinga, 2014). PolyP was initially shown to suppress glyceraldehyde 3-phosphate dehydrogenase (GAPDH) thermal aggregation without noticeable loss in enzymatic activity (Semenyuk *et al.*, 2013) and was recently identified in bacteria as a global, highly effective chaperone, that stabilizes proteins, prevents protein aggregation both *in vitro* and *in vivo*, and maintains proteins in a refolding-competent form (Gray *et al.*, 2014). These results help to explain the long known but largely unexplained role of polyP in protecting bacteria against stress conditions, and suggest that polyP may have served as one of nature's first chaperones (Gray *et al.*, 2014). In contrast, polyP was also shown to have a remarkable efficacy in accelerating amyloid fibril formation, serving as an effective nucleation source for different amyloid proteins, increasing fibril stability and reducing the formation of toxic oligomeric species (Cremers *et al.*, 2016).

In this work, we used biotinylated polyP to identify polyP-binding proteins in lysates from *T. cruzi* and *T. brucei* and were able to identify > 25 proteins in each parasite as putative polyP interaction partners. Among these proteins there was a significant enrichment in nucleolar and glycosomal proteins, which correlated with the cellular localization of polyP in these organelles. Targeting of *Saccharomyces cerevisiae* exopolyphosphatase to the glycosomes of *T. brucei* procyclic forms resulted in polyP hydrolysis, increase in their glycolytic rate and increased susceptibility to oxidative stress.

Results

Lysates of *T. brucei* procyclic forms and *T. cruzi* epimastigotes were incubated with biotinylated polyP after which the polyP-protein complexes were pulled down using magnetic streptavidin-coated beads, followed by washing and elution of bound proteins with high salt buffer. The proteins were identified by mass spectrometry. Two independent experiments for each parasite were done.

We report the proteins that were identified in the two experiments from each parasite (Tables 1 and 2), as well as all the proteins identified in at least one experiment (Tables S1 and S2). Proteins found in samples using biotinylated heparin (another anionic polymer) as control for non-specific binding were subtracted as described under Materials and Methods.

T. brucei *polyP-binding protein identification*

A Mascot search against *T. brucei* Lister 427 database led to the identification of 35 potential polyP-binding proteins identified in both experiments performed, from which 28 have been annotated as putative proteins with a predicted function, and 7 appear as hypothetical proteins (Table 1). The largest groups of identified proteins corresponded to nuclear/nucleolar/ribosomal proteins (13 proteins), and proteins of other or unknown locations (16 proteins), followed by glycosomal proteins (6 proteins). The protein with highest Mascot score in the second experiment was NHP2/RS6-like protein, followed by the glycosomal protein phosphoenolpyruvate carboxykinase (PEPCK), the cytosolic RNA-binding protein (TbAlba2) (Mani *et al.*, 2011), a protein involved in signal transduction (high mobility group protein), and other ribosomal proteins (S15 and L10a), indicating a high relative abundance of these proteins in this proteome.

The list of potential *T. brucei* polyP-binding proteins found in this study is summarized in Table 1, where proteins were grouped by subcellular localization or functional relatedness. Table 1 also includes two additional glycosomal proteins identified in only one of the experiments (labeled with an asterisk). A complete list of *T. brucei* polyP-binding proteins identified in at least one experiment is in Table S1. The distribution according to gene ontology (GO) analysis of the proteins in Table 1 is shown in Fig. S1.

T. cruzi *polyP-binding protein identification*

To identify *T. cruzi* polyP-binding proteins a Mascot search was performed against *T. cruzi* CL Brener (Esmeraldo and non-Esmeraldo like) databases, as the genome sequence of *T. cruzi* Y strain is not yet available.

This search led to the identification of 25 potential polyP-binding proteins found in both experiments, from which 23 have been annotated as putative proteins with a predicted function, and 2 correspond to hypothetical proteins (Table 2).

It is important to mention that additional proteins (31 proteins) were found in *T. cruzi* pull downs but we are reporting here only the ones that were found in both *T. cruzi* experiments (25 proteins). A high number of proteins in *T. cruzi* polyP-binding proteome belong to the group of

Table 1. Polyphosphate-binding proteins identified in *Trypanosoma brucei*.

Mascot score[a]	Protein name	Gene ID[b]	aa[c]	IP[d]
Glycosomal enzymes				
214/473	glycosomal phosphoenolpyruvate carboxykinase	Tb427.02.4210	525	8.75
145/106	hypoxanthine-guanine phosphoribosyl transferase, putative	Tb427.10.1390	234	9.77
165/47	ATP-dependent phosphofructokinase	Tb427.03.3270	487	9.77
69/100	glycerol 3-phosphate dehydrogenase [NAD+], glycosomal	Tb427.08.3530	354	8.75
78/78	fructose-1,6-bisphosphatase	Tb427tmp.211.0540	350	9.46
75/75	glyceraldehyde-3-phosphate dehydrogenase, glycosomal	Tb427.06.4280	359	9.74
74[*]	pyruvate phosphate dikinase	Tb427tmp.02.4150	913	8.82
59[*]	glycerol kinase, glycosomal	Tb427tmp.211.3540	512	8.36
Nuclear/nucleolar/ribosomal proteins				
247/660	NHP2/RS6-like protein	Tb427tmp.160.3670	126	7.37
56/453	ALBA2	Tb427tmp.02.2030	117	9.80
94/401	40S ribosomal protein S15, putative	Tb427.07.2370	172	10.56
22/338	60S ribosomal protein L10a, putative	Tb427tmp.01.1470	214	10.22
74/287	40S ribosomal protein S24E, putative	Tb427.10.7330	137	11.74
138/269	ribosomal protein L36, putative	Tb427.10.1590	109	12.17
133/230	60S ribosomal protein L6, putative	Tb427.10.11390	192	11.05
51/217	40S ribosomal protein S10, putative	Tb427.10.5360	172	10.83
243/162	40S ribosomal protein S8, putative	Tb427.08.6160	220	11.66
187/80	histone H2B, putative	Tb427.10.10460	112	12.29
58/69	histone H3, putative	Tb427.01.2430	133	11.60
60/64	ATP-dependent DEAD/H RNA helicase, putative	Tb427.04.2630	843	10.02
49/18	fibrillarin, putative	Tb427.10.14750	304	10.44
Proteins of other or unknown locations				
155/426	high mobility group protein, putative	Tb427.03.3490	271	10.24
197/162	cyclophilin, putative	Tb427.08.2000	301	10.32
44/118	nascent polypeptide associated complex alpha subunit, putative	Tb427tmp.01.1465	101	10.07
92/80	kinetoplast DNA-associated protein, putative	Tb427.10.8950	126	11.46
88/88	kinetoplast DNA-associated protein, putative	Tb427.10.8890	209	11.33
77/88	acyl-CoA binding protein, putative	Tb427.04.2010	93	10.82
67/67	kinetoplast-associated protein, putative	Tb427.08.7260	1028	10.33
62/62	calmodulin	Tb427tmp.01.4621	149	3.86
42/50	trichohyalin, putative	Tb427tmp.01.3320	658	10.55
69/222	hypothetical protein, conserved[e]	Tb427.03.1820	246	12.03
55/132	hypothetical protein, conserved[f]	Tb427tmp.02.3560	206	12.39
53/64	hypothetical protein, conserved[g]	Tb427tmp.03.0720	174	11.16
60/101	hypothetical protein, conserved	Tb427tmp.01.2800	348	9.99
41/72	hypothetical protein, conserved	Tb427tmp.160.1100	198	11.07
34/53	hypothetical protein, conserved	Tb427tmp.211.4200	337	10.97
94/18	hypothetical protein, conserved	Tb427.10.10030	100	5.04

[a]Mascot scores obtained from search using *T. brucei* Lister 427 database on TriTrypDB (Aslett *et al.*, 2010) in two independent experiments.

[b]Gene identifier from TriTrypDB.

[c]Protein length in amino acids.

[d]Isoelectric point.

[e]The protein is annotated as 'mitochondrial RNA binding complex 1 subunit (Tb927.3.1820)' in the reference strain TREU927 database.

[f]The protein is annotated as 'surfeit locus protein 6 (Tb927.11.5810)' in the reference strain TREU927 database.

[g]The protein is annotated as 'Fcf2 pre-rRNA processing, putative (Tb927.11.420)' in the reference strain TREU927 database.

[*]Glycosomal proteins detected in only one experiment.

nuclear/nucleolar/ribosomal proteins (10 proteins), and proteins of other or unknown location (11 proteins) followed by glycosomal proteins (4 proteins). Mascot scores indicate that the most abundant proteins in this proteome are histidine ammonia-lyase and nucleolar protein 56, followed by fructose-1,6-bisphosphatase. Two other proteins of the gluconeogenesis and glycolysis pathways exhibited a high score (> 300): malate dehydrogenase and 6-phospho-1-fructokinase. Other high-score proteins found in this proteome were: ribosomal proteins L38 and S8, retrotransposon hot spot protein and casein kinase II (Table 2). Some of these high-score proteins were also found in the *T. brucei* polyP-binding proteome, three of them being present in all four *T. brucei* and *T. cruzi* samples analyzed: phosphofructokinase, fructose-1,6-bisphosphatase and ribosomal protein S8. The proteins

Table 2. Polyphosphate-binding proteins identified in *Trypanosoma cruzi.*

Mascot score[a]	Protein name	Gene ID[b]	aa[c]	IP[d]
Glycosomal enzymes				
643/719	fructose-1,6-bisphosphatase, putative	TcCLB.506649.70	344	8.01
108/592	glycosomal malate dehydrogenase, putative	TcCLB.506503.69	323	8.88
148/479	ATP-dependent 6-phosphofructokinase, glycosomal	TcCLB.508153.340	485	9.29
71/108	glyceraldehyde-3-phosphate dehydrogenase, putative	TcCLB.506943.50	359	9.20
36[*]	fructose-bisphosphate aldolase, glycosomal, putative	TcCLB.510301.20	372	8.78
Nuclear/nucleolar/ribosomal proteins				
516/1179	nucleolar protein 56, putative (fragment)	TcCLB.511573.58	387	8.44
527/380	casein kinase II, putative	TcCLB.510761.60	345	8.53
30/553	ribosomal protein L38, putative	TcCLB.503575.34	82	11.09
22/462	40S ribosomal protein S8, putative	TcCLB.511903.110	221	11.41
80/291	snoRNP protein GAR1, putative	TcCLB.510687.120	239	11.92
85/164	fibrillarin, putative	TcCLB.509715.40	316	10.37
78/92	60S ribosomal protein L22, putative	TcCLB.504147.120	130	10.79
56/95	ribosomal protein L36, putative	TcCLB.509671.64	114	12.07
79/76	ribosomal protein S20, putative	TcCLB.508823.120	117	10.52
73/41	small nuclear ribonucleoprotein sm d3	TcCLB.508257.150	115	10.72
Proteins of other or unknown locations				
7900/1379	histidine ammonia-lyase, putative	TcCLB.506247.220	534	8.00
438/503	retrotransposon hot spot (RHS) protein, putative	TcCLB.503483.9	916	8.40
288/180	tripartite attachment complex protein 102	TcCLB.509207.40	1136	5.36
182/53	eukaryotic translation initiation factor 5, putative	TcCLB.504105.20	379	8.24
68/125	serine carboxypeptidase S28, putative	TcCLB.506425.10	631	6.52
76/66	ARP2/3 complex subunit, putative	TcCLB.508737.194	180	7.90
30/85	actin-related protein 2/3 complex subunit 1, putative	TcCLB.504215.40	383	7.61
27/17	ARP2/3 complex subunit, putative	TcCLB.506865.10	328	9.57
63/52	AP-1 medium subunit 1, putative	TcCLB.510533.40	432	7.84
33/102	hypothetical protein, conserved	TcCLB.506857.30	508	7.53
83/28	hypothetical protein	TcCLB.511439.40	455	8.95

[a]Mascot scores obtained from search using *T. cruzi* CL Brener Esmeraldo-like and Non-Esmeraldo-like databases on TriTrypDB (Aslett *et al.*, 2010) in two independent experiments.
[b]Gene identifier from TriTrypDB.
[c]Protein length in amino acids.
[d]Isoelectric point.
[*]Glycosomal protein detected in only one experiment.

glyceraldehyde-3-phosphate dehydrogenase, ribosomal protein L36 and fibrillarin were also found in *T. brucei* and *T. cruzi* samples. Table 2 also includes one additional glycosomal protein identified in only one of the experiments (labeled with an asterisk). Table S2 shows the complete list of *T. cruzi* polyP-binding proteins identified in at least one experiment. The distribution according to gene ontology (GO) analysis of the proteins in Table 2 is shown in Fig. S2.

GO analysis of the polyP-binding partners found a significant overrepresentation of nuclear/nucleolar/ribosomal and glycosomal proteins. We, therefore, investigated whether polyP was localized in these organelles using the polyphosphate-binding domain (PPBD) of *E. coli* exopolyphosphatase (PPX) (Saito *et al.*, 2005). This technique has been used before to localize polyP in yeast (Saito *et al.*, 2005), fungi (Saito *et al.*, 2006), sea urchin eggs

(Ramos *et al.*, 2010), and mast cells (Moreno-Sanchez *et al.*, 2012) vacuoles and myeloma cell nucleoli (Jimenez-Nunez *et al.*, 2012). The original technique (Saito *et al.*, 2005) used the recombinant PPBD of *E. coli* PPX containing an epitope tag at the N-terminal end (Xpress) that was detected with antibodies against the tag. Instead of using a tag and antibodies, we labeled PPBD with Alexa Fluor 488 and directly detected the fluorescence signal of the polyP-bound PPBD.

Localization of polyP in T. brucei

We investigated the localization of polyP in procyclic (PCF) and bloodstream forms (BSF) of *T. brucei* grown in culture using super-resolution structured illumination microscopy. Fig. 1A and B show the staining with Alexa
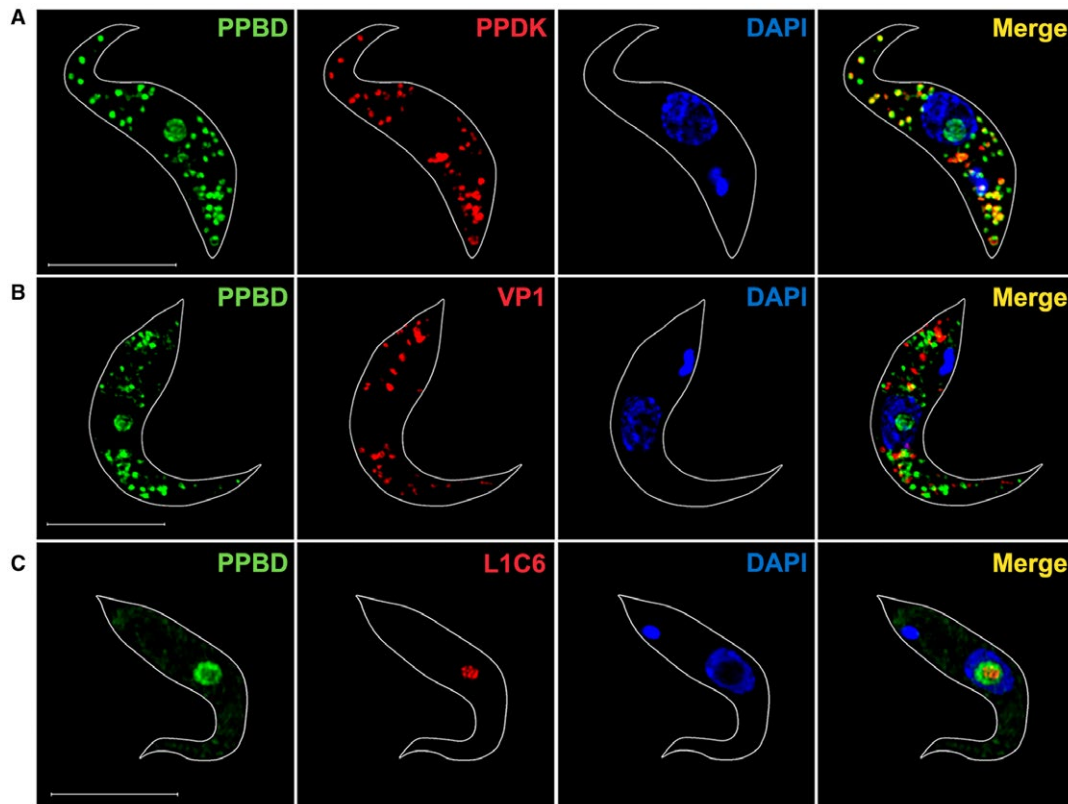
Fig. 1. Super-resolution images of PPBD-labeled *T. brucei* PCF.
A. PPBD (*green*) (8 μg ml^{-1}) localizes in the nucleolus, which is identified as the nuclear region not stained with DAPI (*blue*) and co-localizes (Merge, *yellow*) with antibodies against the pyruvate phosphate dikinase (PPDK, *red*) in the glycosomes.
B. PPBD does not co-localize with antibodies against TbVP1 (*red*), the acidocalcisome marker.
C. PPBD nucleolar localization coincides but does not superimpose to the labeling by nucleolar antibody L1C6 (*red*). The concentration of PPBD used in (C) was lower (2 μg ml^{-1}) to show only nucleolar labeling. Scale bars = 5 μm.

Fluor 488-labeled PPBD of numerous intracellular vesicles randomly distributed in the cytosol of *T. brucei* PCF and staining of the nucleolus, the position of which was identified by the absence of DAPI staining (Landeira and Navarro, 2007). PolyP co-localizes in vesicles with antibodies against glycosomal pyruvate phosphate dikinase (PPDK) (Fig. 1A and Video S1) but not with antibodies against the acidocalcisome vacuolar proton pyrophosphatase (VP1) (Fig. 1B, and Video S2). There was also no co-localization with the mitochondrial marker MitoTracker, or the endoplasmic reticulum marker BiP as detected by immunofluorescence analysis (Fig. S3). The nucleolar localization was also confirmed by co-localization with an unknown nucleolar protein recognized by monoclonal antibody L1C6 (Devaux *et al.*, 2007), which labels an area of the nucleolus distinct from those labeled by DAPI or PPBD (Fig. 1C).

To further demonstrate that the PPBD is detecting longer chain polyP, we pre-incubated it with different concentrations of polyP$_{100}$ and found a concentration-dependent decrease in nucleolar and glycosomal staining in *T. brucei* PCF (Fig. 2A and B). The

nucleolus labeling was abolished when PPBD was pre-incubated with 0.1 and 1 mM (in phosphate units) of polyP$_{100}$. Pre-incubation of PPBD with 1 mM of polyP$_{100}$ reduced overall labeling by approximately 57% in relation to the control. Similarly, pre-incubation with fixed concentrations (1 mM) of longer chain polyP (polyP$_{60}$, polyP$_{100}$ and especially polyP$_{700}$), but not polyP$_3$, prevented labeling of PCF with PPBD (Fig. S4A and B). The labeling of the nucleolus disappeared after pre-incubations of PPBD with polyP$_{60}$, polyP$_{100}$ and polyP$_{700}$. Most effectively, polyP$_{700}$ decreased overall PPBD labeling by almost 78% compared to the control.

In contrast with the results obtained with PCF, there was no labeling of the BSF nucleoli with PPBD and only partial co-localization with the glycosomal marker PPDK (Fig. 3A). However, as occurs with PCF, there was no co-localization of PPBD with VP1 in BSF (Fig. 3B).

Localization of polyP in *T. cruzi*

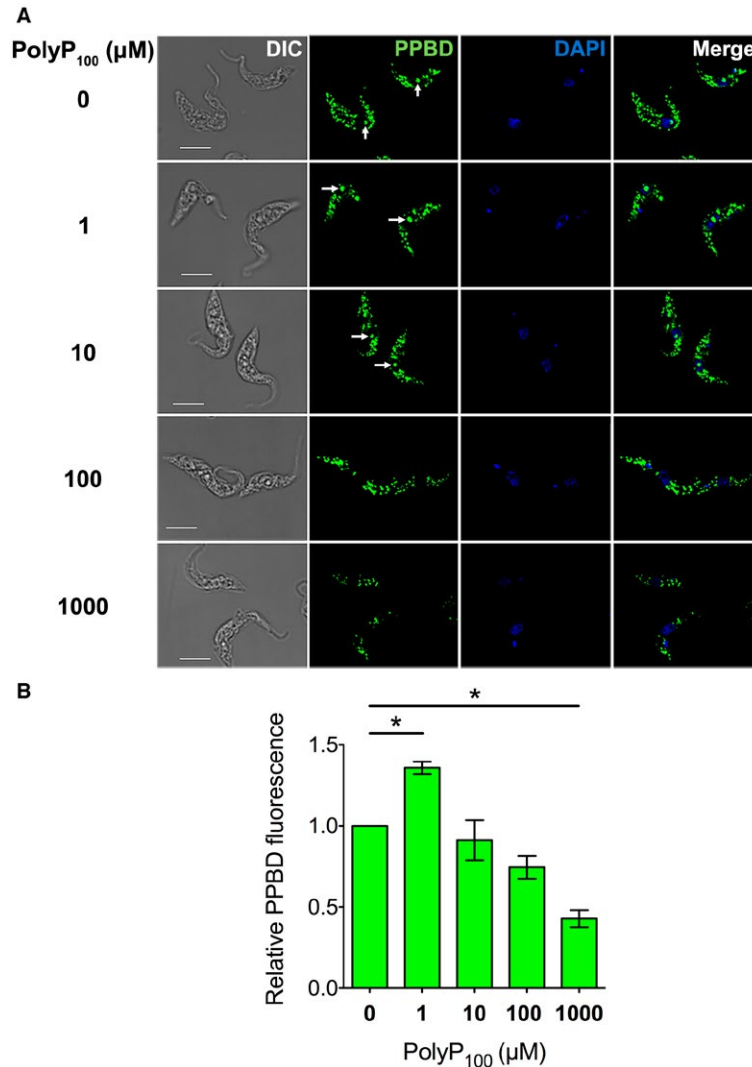We also investigated the localization of polyP in *T. cruzi* using PPBD. Fig. 4A and B show a strong nucleolar

Fig. 2. Fluorescence microscopy analysis of the effect of different concentrations of polyP$_{100}$ on PPBD staining in *T. brucei* PCF.
A. PPBD (*green*) was pre-incubated with 0–1.0 mM polyP$_{100}$ (in phosphate units) for 1 h and then cell labeling was analyzed by fluorescence microscopy. Nucleolus labeling is indicated by *white arrows*. Differential interference contrast (DIC) images are shown on the left panel. DAPI staining is in *blue*. Scale bars = 5 μm.
B. Quantification of the fluorescence of cells labeled with PPBD previously incubated with polyP$_{100}$ as compared with control cells. A total of 471 cells were examined in three biological experiments. Values are means ± SEM (*n* = 3), * $P < 0.05$, One-Way ANOVA test with multiple comparisons.

staining of epimastigotes with PPBD and a weak cytosolic staining that did not co-localize with antibodies against PPDK (Fig. 4A) or VP1 (Fig. 4B). Although cytosolic staining appears punctate this is because super-resolution microscopy eliminates the fluorescence coming from regions occupied by organelles, but this pattern is not apparent in regular fluorescent images (Fig. S5). In contrast, *T. cruzi* trypomastigotes (Fig. 4C and D) and amastigotes (Fig. 4E and F) showed strong nucleolar localization, partial co-localization with the glycosomal marker PPDK, and no co-localization with VP1.

Detection of long-chain polyP in isolated glycosomes and acidocalcisomes

We isolated glycosomes and acidocalcisomes by a modification of an isolation procedure described previously (Huang *et al.*, 2014). After grinding with silicon carbide to break the cells, the lysates were fractionated by differential centrifugation followed by density-gradient ultracentrifugation using high-density solutions of iodixanol (Fig. S6). The crude glycosomal fraction obtained from the first iodixanol gradient was applied to the 27% step of the second iodixanol gradient resulting in seven fractions. Fig. 5 shows protein abundance
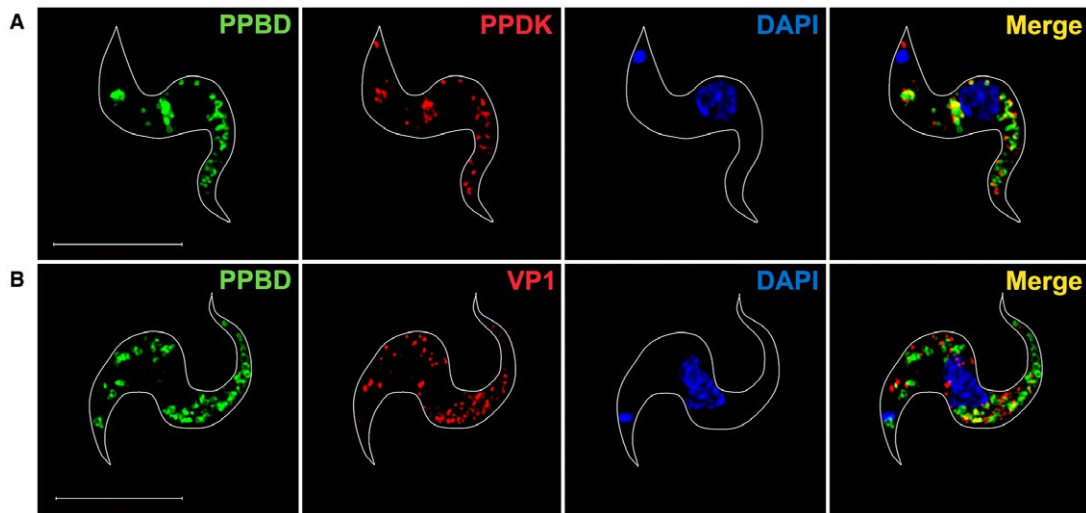
Fig. 3. Super-resolution images of PPBD-labeled *T. brucei* BSF.
A. PPBD (*green*) does not label the nucleolus and partially co-localizes (Merge, *yellow*) with antibodies against PPDK (*red*).
B. PPBD does not co-localize with antibodies against TbVP1 (*red*). DAPI staining is in *blue*. Scale bars = 5 μm.

(Fig. 5A) as well as distribution of markers for glycosomes (hexokinase) (Fig. 5B) and acidocalcisomes (aminomethylenediphosphonate (AMDP)-sensitive vacuolar pyrophosphatase activity, TbVP1) (Fig. 5C). Glycosomes were enriched in fractions 1 and 2, while acidocalcisomes were enriched in fractions 3 and 5. We also evaluated our purification method by western blot analyses of the fractions using antibodies against a glycosomal marker (*T. brucei* pyruvate phosphate dikinase [TbPPDK]) and an acidocalcisomal marker (TbVP1). The crude glycosomal fraction (C) showed contamination with the acidocalcisome marker. However, fractions 1 and 2 of the second gradient were free of TbVP1 antibody reaction (Fig. 5D). Some pyrophosphatase activity was detected in fraction 2 (Fig. 5C) but since no antibody reaction was detected (Fig. 5D) it can be attributed to the soluble inorganic pyrophosphatase described in trypanosomatids (Gomez-Garcia *et al.*, 2004) or other non-specific pyrophosphatase activity. Fractions 1 and 2, or the acidocalcisome fractions obtained in the first iodixanol gradient (Fig. S6) were pooled and extracted for polyP analyses. Long-chain polyP assayed by 30% polyacrylamide gel electrophoresis (PAGE), and staining with toluidine blue, showed the presence of long-chain polyP in both glycosomal and acidocalcisomal fractions (Fig. 5E).

Expression of S. cerevisiae *PPX in the glycosomes and* E. coli *PPX in the nuclei of* T. brucei *and phenotypic changes detected*

To decrease the amount of polyP in PCF glycosomes, we expressed *S. cerevisiae* PPX1 (ScPPX1), which specifically hydrolyzes polyP to inorganic phosphate (Wurst and Kornberg, 1994), fused to a glycosomal targeting sequence (peroxisome-targeting sequence 2 [PTS2]) and enhanced yellow fluorescent protein (eYFP) (Bauer *et al.*, 2013). The plasmid integrates into the tubulin locus and the procyclin repetitive acidic protein promoter (PARP) drives its constitutive expression (Bauer *et al.*, 2013). Expression of PTS2-ScPPX1-eYFP in glycosomes was confirmed by fluorescence microscopy. Figure 6A shows co-localization of the green fluorescent signal from the expressed protein with antibodies against PPDK, a glycosomal marker. Western blot analysis confirmed the expression of the protein (Figs 6B and S7). We confirmed the activity of the expressed enzyme by measuring levels of P_i of cell lysates from cells transfected with the plasmid as compared to those of lysates from wild type cells. PolyP is very abundant in the cells and upon lysis it is released from different cellular compartments together with the glycosomally targeted ScPPX. When the lysates were incubated at 30°C there was an increase in the PPX activity of lysates from *PTS2-ScPPX1-eYFP*-expressing cells when compared to the endogenous PPX activity of lysates from WT cells (Fig. 6C) but this activity did not increase by adding exogenous polyP$_{100}$ indicating that there was enough polyP in the medium to saturate the enzyme released from the glycosomes.

To establish whether expression of ScPPX resulted in a decrease in polyP, we measured total short- and long-chain polyP in wild type and *PTS2-ScPPX1-eYFP*-expressing cells using a biochemical method based on the P_i release by recombinant ScPPX, but we did not observe significant differences (Fig. S8). However,
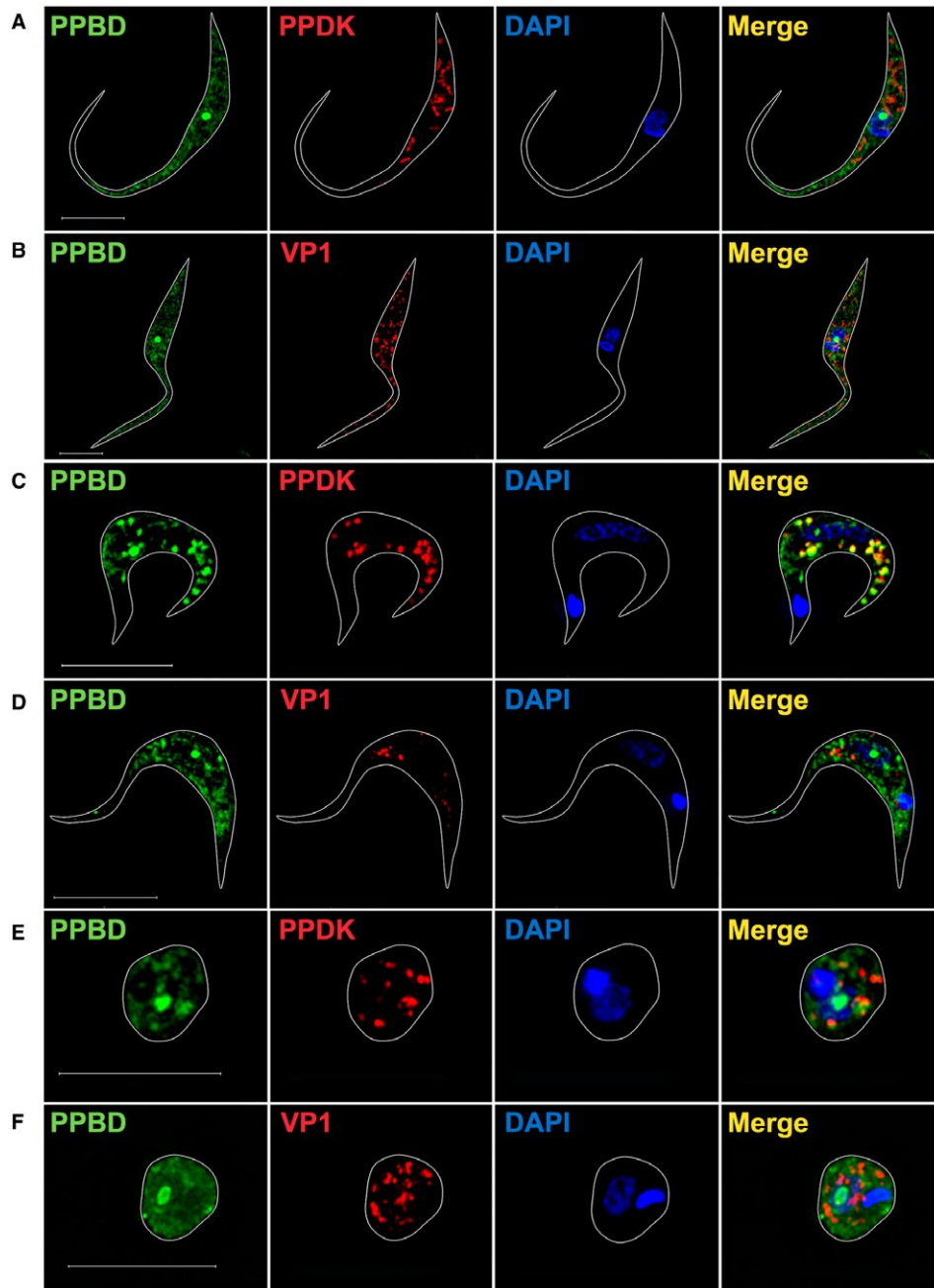
Fig. 4. Super-resolution images of PPBD-labeled *T. cruzi*.

A, B. In epimastigotes PPBD (*green*) labels the nucleolus and shows diffuse cytosolic labeling that does not co-localize (Merge, *yellow*) with antibodies against PPDK (*red*) (A) or with antibodies against TbVP1 (*red*) (B). Scale bars = 5 μm.

C, D. In trypomastigotes, PPBD labels the nucleolus and partially co-localizes (Merge, *yellow*) with antibodies against PPDK (*red*) (C) but not with antibodies against TbVP1 (*red*) (D). Scale bars = 5 μm.

E, F. In amastigotes, PPBD labels the nucleolus and partially co-localizes (Merge, *yellow*) with antibodies against PPDK (*red*) (E) but not with antibodies against TbVP1 (*red*) (F). DAPI staining is in *blue*. Scale bars = 5 μm.

when we measured short-chain polyP by 35.5% PAGE, toluidine blue staining revealed a higher accumulation of short-chain polyP (lower than 60 P_i units) in *PTS2-ScPPX1-eYFP*-expressing cells as compared to wild type cells. These results are consistent with the hydrolysis of

long-chain polyP by glycosomally targeted ScPPX (Fig. 6D and E).

T. brucei PCF expressing glycosomal PPX grew at the same rate as control cells (Figs 6F and S9). However, glucose consumption of *PTS2-ScPPX1-eYFP*-expressing
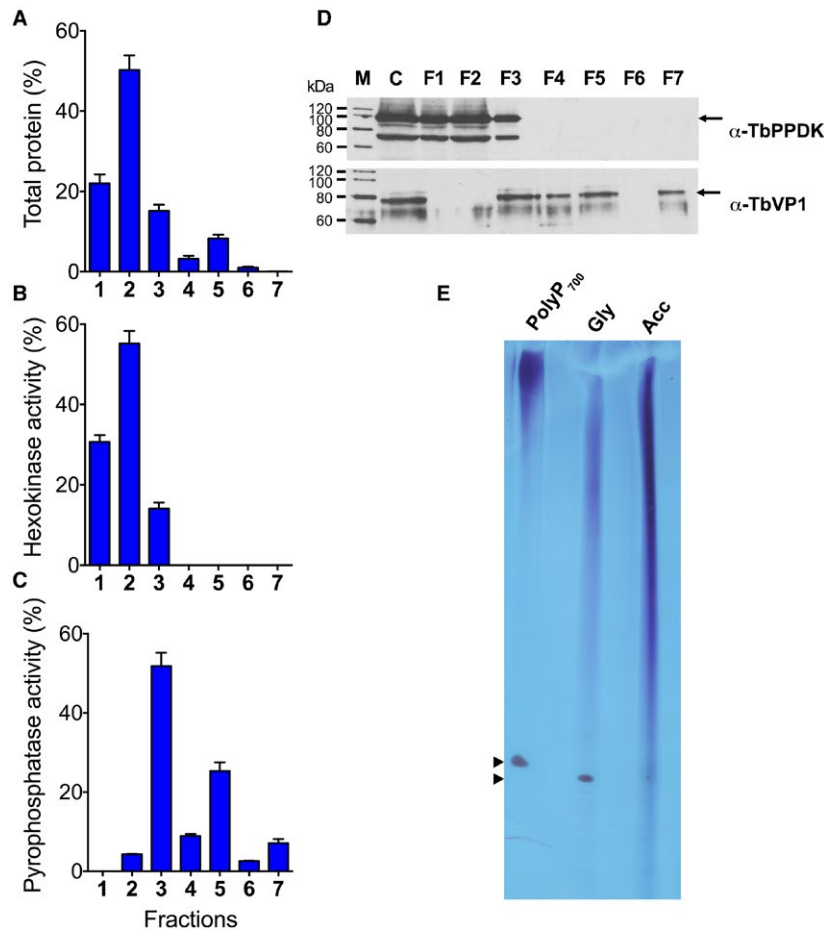
Fig. 5. Distribution on iodixanol gradients of organellar markers from wild-type PCF trypanosomes and detection of long-chain polyP.
A. Protein distribution.
B. Glycosomal marker (hexokinase) distribution.
C. Acidocalcisomal marker (pyrophosphatase) distribution. In (A–C), the *y*-axis indicates relative distribution; the *x*-axis indicates fraction number from wild-type *T. brucei* PCF; *bars* show means ± SD from three independent experiments. In (B–C) the values are expressed as a percentage of the total recovered activity.
D. Western blot analyses done with aliquots of fractions from wild-type *T. brucei* PCF, using antibodies against the glycosomal protein marker TbPPDK or the acidocalcisomal protein marker TbVP1, as described under Materials and Methods. C, crude glycosomes from the first iodixanol gradient. F1–F7, fractions from the second iodixanol gradient, as indicated in Fig. S6. Molecular weight markers (M) and antibodies are shown at left and at right, respectively. Arrows show the bands corresponding to TbPPDK and TbVP1.
E. Long-chain polyP as detected by PAGE. Long-chain polyP was extracted from glycosome (Gly) and acidocalcisome (Acc) subcellular fractions (Fig. S6). PolyP$_{700}$ was used as a marker. Arrowheads indicate the orange G dye used in the sample buffer.

cells after 6 h of incubation in culture medium was higher (Fig. 6G), and these cells were more sensitive to oxidative stress than control cells (Fig. 6H).

To decrease the levels of polyP in the nucleolus we tried to target *E. coli* PPX (EcPPX) to the nucleolus using a nucleolar localization signal (NoLS) reportedly used to target GFP to this organelle in *T. brucei* (Hoek *et al.*, 2000). Expression of the protein NoLS-EcPPX-GFP was confirmed by western blot analysis (Fig. 7A) and it had nuclear but not nucleolar localization and failed to decrease PPBD staining of nucleolar polyP (Fig. 7B).

Discussion

Inorganic polyP has multiple functions in both bacteria and eukaryotes. Some of these functions can be attributed to its chemical properties, such as its ability to store phosphate in an osmotically neutral form, to bind and store organic and inorganic cations, to store energy in the form of a few to hundreds of phosphoanhydride bonds, to combine with other polymers for the formation of channels and pumps, or to act as inorganic chaperone of proteins (Kornberg, 1995; Moreno and Docampo, 2013; Gray *et al.*, 2014). Other more complex functions, however, such as its role in transcriptional control, and
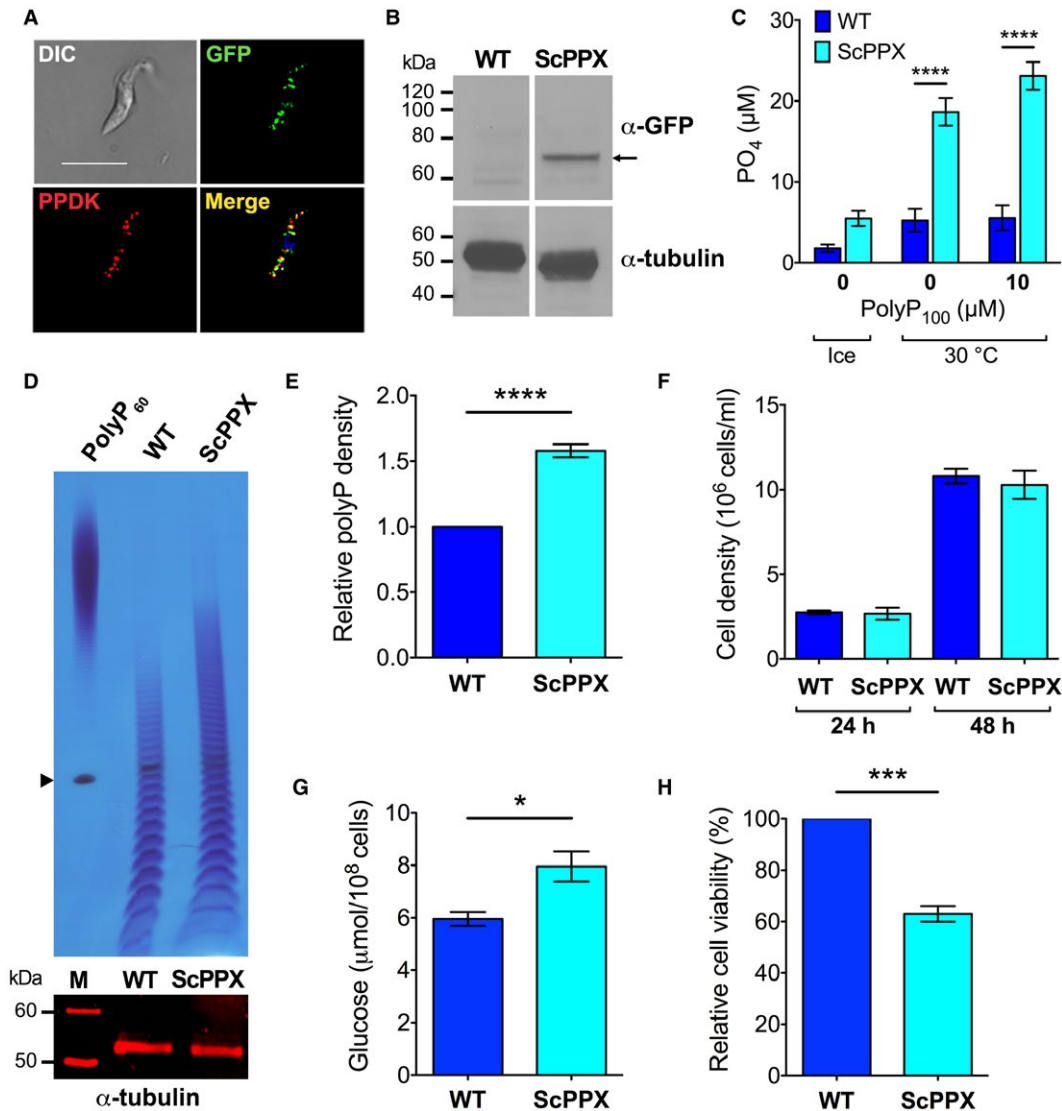
Fig. 6. Glycosomal expression of ScPPX in *T. brucei* PCF and resulting phenotypic changes.

A. PTS2-ScPPX1-eYFP (*green*) co-localizes (Merge, *yellow*) with antibodies against PPDK (*red*) (Pearson's correlation coefficient = 0.5726). DIC, differential interference contrast. DAPI staining is in *blue*. Scale bar = 5 µm.

B. Western blot analysis of PCF WT and *PTS2-ScPPX1-eYFP*-expressing cells using polyclonal antibody against GFP. Molecular weight markers are at *left* and *arrow* shows the band corresponding to PTS2-ScPPX1-eYFP (expected size: ~ 73 kDa). Tubulin was used as a loading control. Full gel in shown in Fig. S7.

C. Exopolyphosphatase assays in lysates. Lysates (4.5×10^7 cell equivalents) of WT or *PTS2-ScPPX1-eYFP*-expressing cells were incubated in ice or at 30°C for 10 min in the absence or presence of 10 µM polyP$_{100}$ (in phosphate units). ScPPX means *PTS2-ScPPX1-eYFP*-expressing cells. Values are means ± SEM ($n = 3$), *****$P < 0.0001$. Two-way ANOVA test with multiple comparisons.

D. Short chain polyphosphate as detected by PAGE. Short-chain polyP was extracted from WT and *PTS2-ScPPX1-eYFP*-expressing cells. PolyP$_{60}$ was used as a marker. Arrowhead indicates orange G dye. Tubulin was used as a loading control.

E. Densitometry of toluidine stained polyP from WT and *PTS2-ScPPX1-eYFP*-expressing cells. Values are means ± SEM ($n = 4$), *****$P < 0.0001$. Student's *t*-test.

F. Growth of WT or *PTS2-ScPPX1-eYFP*-expressing cells at 24 and 48 h. No significant differences observed, $n = 3$.

G. Glucose consumption in WT and *PTS2-ScPPX1-eYFP*-expressing cells after 6 h of incubation in culture medium at high cell density (10^8 cells ml^{-1}). Values are means ± SEM ($n = 3$), *$P < 0.05$. Student's *t*-test.

H. Percentage of live cells following 24 h-incubation after treatment with 50 µM H$_2$O$_2$ for 1 h at 28°C. Values are means ± SEM ($n = 3$), ****$P < 0.001$. Student's *t*-test.

regulation of enzyme activity, motility or resistance to stress response might depend on its interaction with proteins and cell signaling (Rao *et al.*, 2009). However,

besides its interaction with proteins of the blood coagulation cascade (Smith *et al.*, 2006), or its ability to polyphosphorylate proteins (Azevedo *et al.*, 2015;
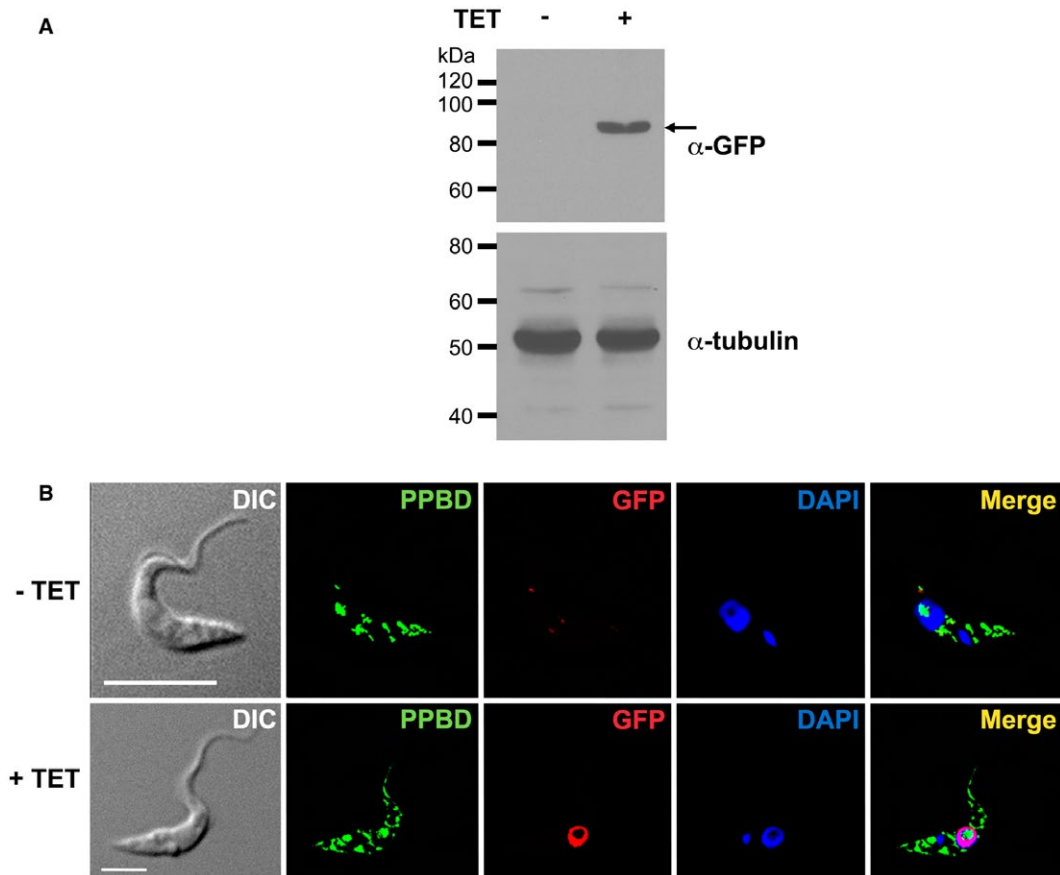
Fig. 7. Western blot analysis and fluorescence microscopy of *NoLS-EcPPX-GFP*-expressing *T. brucei* PCF.
A. Western blot analysis of uninduced (–TET) and induced (+TET) *T. brucei* PCF transfected with an expression vector containing EcPPX-GFP with a NoLS using polyclonal antibody against GFP. Molecular weight markers are at *left* and *arrow* shows the band corresponding to NoLS-EcPPX-GFP (expected size: ~ 89 kDa). Tubulin was used as a loading control.
B. Uninduced (–TET) and induced (+TET) *T. brucei* PCF transfected with NoLS-EcPPX-GFP plasmid were subjected to immunofluorescence analysis. Parasites were labeled with PPBD (*green*), antibodies anti-GFP (*red*) and DAPI (*blue*). Differential interference contrast (DIC) images are shown on the left panel. Merged images are shown on the right panel. In induced cells, EcPPX (*red*) exhibits nuclear localization and does not co-localize with nucleolar PPBD (*green*). Scale bars = 5 μm. TET: tetracycline.

Bentley-DeSousa *et al.*, 2018), little is known of other interactions with cellular proteins. Our proteomic studies are a first step in the identification of polyP-interacting proteins in eukaryotes.

The proteomic studies of polyP-binding proteins revealed an overrepresentation of nucleolar and glycosomal proteins in both *T. cruzi* and *T. brucei* and these results correlated with the localization of the polymer to the nucleolus and glycosomes. Interestingly, known polyP-associated proteins such as the components of the vacuolar transporter chaperone (VTC) complex involved in its synthesis (Fang *et al.*, 2007a; Lander *et al.*, 2013; Ulrich *et al.*, 2014) and the PPX (Fang *et al.*, 2007b) and vacuolar soluble pyrophosphatase (VSP) (Lemercier *et al.*, 2004; Yang *et al.*, 2016), involved in its degradation, were not identified among the interacting partners. This could be explained because these enzymes are involved in short-chain polyP synthesis and degradation

while we used long-chain polyP bound to biotin for the pull downs.

Besides several glycolytic enzymes (phosphofructokinase, fructose-bisphosphate aldolase, GAPDH) other glycosomal enzymes (PEPCK, malate dehydrogenase, pyruvate phosphate dikinase, fructose 1,6-bisphosphatase, glycerol 3-phosphate dehydrogenase, glycerol kinase, hypoxanthine-guanine phosphoribosyl-transferase [HGPRT]) were present in the pull downs. Multiple nuclear and nucleolar proteins (ribosomal subunits, snoRNP protein GAR1, small nucleolar ribonucleoprotein SmD3, fibrillarin, histones, high mobility group protein, casein kinase 2) were also detected. These results are in agreement with the localization of polyP in the nucleolus and glycosomes of the parasites. Interestingly, not all PPDK-stained glycosomes were detected by PPBD staining and many PPBD-positive particles were not recognized by

anti-PPDK, suggesting the possibility of different populations of glycosomes.

The first report of the presence of PPDK in *T. brucei* (Bringaud *et al.*, 1998) showed that the enzyme was not detectable in long slender BSF trypanosomes of Lister 427 or GUTat strain grown in rats and that short stumpy forms of GUTat strain grown in mice had low expression levels, as detected by western blot analyses. No PPDK was detected by immunofluorescence analysis of BSF trypanosomes. Our results suggest that either the BSF trypanosomes grown in culture that we used have stumpy-like characteristics or that the antibody we used was able to detect this enzyme using our standard IFA protocol.

It is interesting to note that many glycosomal proteins have the highest calculated positive charge within its family of homologous proteins (Wierenga *et al.*, 1987). These observations led some authors to postulate the presence of 'hot spots' of basic amino acids about 40 Å apart that could be important for the glycosomal import of these proteins (Wierenga *et al.*, 1987). This idea was later discarded but the reason for the high positive charge of these proteins is still puzzling. It is tempting to speculate that polyP is the scaffold that maintains the tight packing of the glycosomal enzymes (Michels *et al.*, 2000), and could be involved in the transfer of the negatively charged glycolytic intermediates between the enzymes.

Another potential reason for the highest glycolytic rate of parasites targeted with ScPPX to the glycosomes is an inhibitory effect of polyP or a stimulatory effect of its hydrolytic products (Pi and PPi) on glycolytic activities. Glycosomes contain enzymes that can be inhibited by PPi such as the hexokinases of *T. cruzi* (Caceres *et al.*, 2003) and *L. mexicana* (Pabon *et al.*, 2007), one of the hexokinases of *T. brucei* (Chambers *et al.*, 2008), and the PEPCK of *T. cruzi* (Acosta *et al.*, 2004), but their inhibition by polyP has not been tested. On the contrary, binding of glycosomal enzymes to polyP could be explained by the presence of binding domains to polyP. Several glycosomal enzymes found in our proteome analyses, like HGPRT (Shih *et al.*, 1998) and pyruvate phosphate dikinase (PPDK) (Bringaud *et al.*, 1998; Shih *et al.*, 1998; Maldonado and Fairlamb, 2001) produce or utilize PPi. Phosphofructokinase (PFK) is an ATP-dependent enzyme but shows a high degree of sequence and structural similarity with PPi-dependent enzymes (Michels *et al.*, 1997; McNae *et al.*, 2009; Rodriguez *et al.*, 2009). Thus, interaction with potential PPi- or polyP-binding sites could explain their pull down by polyP. PolyP anions have been involved in stabilization of GAPDH (Semenyuk *et al.*, 2013), another glycolytic enzyme found in both polyP-binding proteomes. In that work, the authors demonstrated that polyP suppresses thermal aggregation of the enzyme without affecting its activity. This could be a general mechanism for polyP-mediated regulation of glycolytic enzymes and it could explain the presence of polyP in *T. brucei* and *T. cruzi* glycosomes. Our results indicate that a detailed analysis of the effect of polyP on glycosomal enzymatic activities is warranted.

PolyP has been found in most subcellular compartments investigated so far but this is the first report of its presence in a peroxisome-related organelle. As glycosomes share not only similar biogenesis mechanisms, morphology, and some metabolic processes, but also have in common a dense matrix of proteins with P_i values on average 1–2 pH unit higher than those in the cytosol (Michels and Opperdoes, 1991; Gabaldon *et al.*, 2016), it is possible that polyP is present in peroxisomes of other organisms. In this regard, it has been indicated that peroxisomes seem to entirely lack proteinaceous chaperones and that it will be intriguing to test how the polyP pathway might play a role in the development of stress resistance in these organelles (Kampinga, 2014).

Only one polyP-synthesizing activity has been described in trypanosomes, which is catalyzed by the acidocalcisomal VTC complex (Lander *et al.*, 2013). However, conditional knockout of VTC4, the catalytic subunit of the complex, in *T. brucei* did not affect the levels of long-chain polyP suggesting the involvement of other enzymes in its synthesis (Ulrich *et al.*, 2014). It is currently unknown whether polyP is synthesized within glycosomes or reach the organelles by piggy-backing on the glycosomal matrix enzymes that are synthesized in the cytosol and post-translationally imported via transient pores or by non-selective pores such as those that have been detected in *T. brucei* glycosomal (Gualdron-Lopez *et al.*, 2012) or in different organisms peroxisomal (Antonenkov and Hiltunen, 2012) membranes. In contrast, it has been reported that several NUDIX hydrolases in yeast and humans (Lonetti *et al.*, 2011) possess polyP degrading activity and at least two NUDIX hydrolases (TbNH2 and TbNH3) have been detected in the glycosome proteome (Guther *et al.*, 2014). Work is in progress to investigate their activity.

The interaction of polyP with ribosomal proteins has been previously reported in *E. coli* for two main processes: degradation of ribosomal protein through polyP-Lon protease complex (Kuroda *et al.*, 2001) and as promoter of translation fidelity (McInerney *et al.*, 2006). The ATP-dependent Lon protease forms a complex with polyP that degrades most of the ribosomal proteins, thereby supplying the amino acids required for response to starvation (Kuroda *et al.*, 2001). In contrast, polyP interacts with ribosomes to maintain optimal translation efficiency, as demonstrated in experiments measuring the *in vivo* translation rate in polyP kinase (*ppk*) mutants (McInerney *et al.*, 2006). These studies provide an explanation for the abundance of ribosomal proteins observed in *T. brucei* and *T. cruzi* polyP-binding proteomes.

Transcription factors and RNA binding proteins represent another significant functional group in the *T. brucei* and *T. cruzi* polyP-binding proteomes. A previous work reported a role for polyP in transcription of myeloma plasma cells, where they accumulate higher levels of nucleolar polyP than normal plasma cells (Jimenez-Nunez *et al.*, 2012). In that work, they confirmed that nucleolar RNA polymerase I was modulated by polyP, opening up a broad spectrum of possibilities regarding the role of polyP as regulator of gene expression at the transcriptional level. In fact, another nucleolar enzyme that appeared with high score in *T. cruzi*, and also with a lower score in the *T. brucei* polyP-binding proteome, was the casein kinase II alpha subunit (CK2α). This enzyme has been characterized in *T. brucei* and it accumulates in the nucleolus, which is the site of ribosome biogenesis and where many of the CK2 substrates are present (Park *et al.*, 2002). This isoform of the catalytic subunit prefers ATP over GTP as a substrate and modulators of its function are still unknown. It would be interesting to evaluate whether polyP regulates CK2 activity, as the anionic polymer and the enzyme localize to the nucleolus and are involved in transcription regulation. The report that many nucleolar proteins can be polyphosphorylated (Bentley-DeSousa *et al.*, 2018) supports the presence of this polymer in the nucleoli.

Most polyP in trypanosomatids have been proposed to be concentrated in acidocalcisomes (Docampo, 2016). Early ^{31}P-NMR studies of isolated acidocalcisomes from *T. brucei* PCF and *T. cruzi* epimastigotes found that the average chain lengths of polyP are 3.39 and 3.25 (Moreno *et al.*, 2000), respectively, values that were in good agreement with the average phosphate chain lengths determined by X-ray microprobe analysis in *T. cruzi* (Scott *et al.*, 1997; Moreno *et al.*, 2000). This was considered consistent with the ability of the acidocalcisomal recombinant Vtc4 to synthesize short-chain polyP *in vitro* (Lander *et al.*, 2013). However, subcellular fractionation of *T. cruzi* epimastigotes detected both short- and long-chain polyP in acidocalcisome fractions (Ruiz *et al.*, 2001). In this work, we confirmed that acidocalcisomes, like glycosomes, possess considerable amounts of long-chain polyP (Fig. 5E). This apparent discrepancy could be explained by the difficulty in detecting long-chain polyP by ^{31}P-NMR because of its broad signal, and the potential need of a membrane potential to efficiently synthesize and translocate long-chain polyP in intact vacuoles (Hothorn, 2009), in contrast to the *in vitro* synthesis by the recombinant enzyme. Acidocalcisomes, however, were not stained by PPBD. One potential explanation is that this highly charged polymer is known to bind Mg^{2+} and other cations in acidocalcisomes and form gels (Klompmaker *et al.*, 2017) that could be inaccessible to PPBD. This might not occur in the glycosomes and nucleolus where polyP could be associated with proteins leaving free negatively

charged residues that could more easily bind to PPBD. *In vitro* competitive binding assays previously showed that PPBD binds strongly to free long-chain polyP and has been described as a reliable method for long-chain polyP detection (Saito *et al.*, 2005). Long-chain polyP is very abundant in different trypanosomatids with reported values of 2.9, 0.8 and 0.13 mM in *T. cruzi* epimastigotes, trypomastigotes and amastigotes, respectively (Ruiz *et al.*, 2001); 57 mM in *Leishmania major* promastigotes (Rodrigues *et al.*, 2002), and 6 mM in *T. brucei* procyclic forms (Lemercier *et al.*, 2002).

We were not able to detect significant differences in short- and long-chain polyP content of total lysates from wild type and *PTS2-ScPPX1-eYFP*-expressing *T. brucei* procyclic forms. Therefore, we assayed polyP by PAGE in total cell extracts and we detected an increase in short-chain polyP in *PTS2-ScPPX1-eYFP*-expressing cells. The results could be explained if only the glycosomal long-chain polyP is hydrolyzed in *PTS2-ScPPX1-eYFP*-expressing cells, resulting in the increase in polyP of less than 60 P_i units, with no apparent decrease in short- and long-chain polyP levels in total cell extracts.

Our results using the PPBD of *E. coli* PPX suggest that the nucleolus and glycosomes possess long-chain polyP. Targeting of yeast PPX to glycosomes of *T. brucei* resulted in decreased cellular polyP levels, alteration in their glycolytic flux, and increase in the susceptibility to oxidative stress. It is interesting to note that *T. cruzi* glycosomes only possess a glutathione peroxidase I, which decomposes hydroperoxides but not H_2O_2 (Wilkinson *et al.*, 2002), and that polyP has been shown to protect cells from oxidative stress (Gray *et al.*, 2014).

The nucleoli are membrane-less RNA/protein bodies within the nucleus where they function in ribosome subunit biogenesis. Despite the knowledge gained on their function, there is still some lack of understanding of what holds the RNA and protein components together as a physical structure (Brangwynne *et al.*, 2011). Recent evidence suggests that they have liquid-like properties, with an effective surface tension that minimizes surface area by viscous relaxation to a spherical shape and that may assemble by intracellular phase separation (Brangwynne *et al.*, 2011). The nucleation properties of polyP (Cremers *et al.*, 2016) could have a role in phase separation and RNA-protein interactions.

Targeting of *E. coli* PPX to the nucleolus did not reduce PPBD staining suggesting that nucleolar polyP could not be hydrolyzed because the enzyme could not localize to the nucleolus. The liquid droplet-like behavior of nucleoli could make them inaccessible to the enzymatic activity of EcPPX. In this regard, overexpression of EcPPX in yeast was also unable to reverse polyphosphorylation of target proteins (Bentley-DeSousa *et al.*, 2018). Another possible explanation could be the reported masking of some polyP chains, which makes them resistant to the

hydrolytic action of PPXs (Rao *et al.*, 2009). In this regard, derivatization of the terminal phosphates of polyP conferred resistance to PPX digestion (Choi *et al.*, 2010). Furthermore, it has been suggested (Saiardi, 2012) that inositol hexakisphosphate (IP$_6$) could be at the edge of polyP acting as a cap, like the one protecting mRNA for degradation, and protect polyP from the action of PPXs.

In conclusion, our work reveals a novel localization of polyP to the glycosomes and nucleolus of trypanosomatids and that hydrolysis of glycosomal polyP results in an increased glycolytic rate and increased susceptibility to oxidative stress.

Experimental procedures

Chemicals and reagents

Monoclonal antibody L1C6 (Devaux *et al.*, 2007) was provided by Dr. Keith Gull (Oxford University, UK), polyclonal antibody against TbBiP (Bangs *et al.*, 1993) was provided by Dr. Jay Bangs (University at Buffalo, NY), polyclonal rabbit antibody against TbVP1 (Lemercier *et al.*, 2002) was provided by Dr. Norbert Bakalara (University of Montpellier, France), monoclonal antibody against *T. brucei* pyruvate phosphate dikinase (TbPPDK) (Bringaud *et al.*, 1998) was provided by Dr. Frédéric Bringaud (University of Bordeaux, France), the pXS2-AldoPTS2-eYFP vector (Bauer *et al.*, 2013) was provided by Dr. Meredith T. Morris (Clemson University, NC), pTrc-PPBD plasmid (Saito *et al.*, 2005) was provided by Dr. Katsuharu Saito (Shinshu University, Nagano-Ken, Japan) and pLEW100v5bld-BSD plasmid was provided by Dr. George Cross. PolyP$_{60}$ was provided by Dr. Toshikazu Shiba (RegeneTiss Inc., Okaya, Japan). PolyP$_3$ (Na$_5$P$_3$O$_{10}$) was from Sigma-Aldrich (St. Louis, MO), and polyP$_{100}$ and polyP$_{700}$ were from Kerafast (Boston, MA). AMDP was synthesized by Michael Martin (University of Illinois at Urbana-Champaign). Slide-A-Lyzer Dialysis Cassette, HisPur Ni-NTA Chromatography Cartridge and Slide-A-Lyzer Dialysis Cassette were from Thermo Scientific (Thermo Fisher Scientific, Walthman, MA). Alexa Fluor 488 Microscale Protein Labeling kit, MitoTracker Red CMXRos and rabbit anti-GFP antibody were from Invitrogen Molecular Probes (Eugene, OR). Rabbit anti-HA was from Abcam (Cambridge, MA). Dynabeads MyOne Streptavidin T1 beads, blasticidin S HCL, and hygromycin B were from Invitrogen (Carlsbad, CA). Biotinylated heparin (Cat. No. 375054) was from Merck (Millipore Sigma, Burlington, MA). BCA Protein Assay kit and ECL Western Blotting Substrate were from Pierce Protein Biology (Thermo Fisher Scientific, Walthman, MA). Phusion High-Fidelity DNA polymerase and restriction enzymes were from New England Biolabs (Ipsich, MA). In-Fusion HD Cloning kit, and *E. coli* Stellar Competent Cells were from Clontech Laboratories (Mountain View, CA). Zymo 5α Mix & Go competent cells was from Zymo Research (Irvine, CA). LigaFast Rapid DNA Ligation System was from Promega (Madison, WI). G418 was from KSE Scientific (Durham, NC). Fluoromount-G mounting medium was from Southern Biotech (Homewood, AL). Benzonase was from Novagen (Merck Millipore, Burlington, MA). Mini-PROTEAN TGX Precast Protein Gel was from BioRad (Hercules, CA). MagicMark XP Western Protein Standard was from Life Technologies (Carlsbad, CA). D-Glucose Assay Kit (GOPOD Format) was from Megazyme Inc. (Chicago, IL). Protease inhibitor cocktail for use in purification of histidine-tagged proteins (Cat. No. P8849), protease inhibitor cocktail for use with mammalian cell and tissue extracts (Cat. No. P8340), polyclonal rabbit anti-tubulin and anti-IgG antibodies and all other reagents of analytical grade were from Sigma-Aldrich (St. Louis, MO).

Cell cultures

For most studies, *T. brucei* PCF and BSF (Lister 427) were grown as reported previously (Lander *et al.*, 2013; Huang *et al.*, 2014). Cell density was verified by counting parasites in a Neubauer chamber. *PTS2-ScPPX1-eYFP*-expressing PCF were grown in the presence of 10 μg ml^{-1} blasticidin. *NoLS-EcPPX-GFP*-expressing PCF were grown in the presence of 15 μg ml^{-1} G418, 50 μg ml^{-1} hygromycin, and 10 μg ml^{-1} blasticidin. For proteomic studies, *T. brucei* PCF (29-13 strain) were grown at 28°C in SM medium (Cunningham and Honigberg, 1977) supplemented with 10% heat-inactivated fetal bovine serum (FBS), 8 μg ml^{-1} hemin, 15 μg ml^{-1} G418 and 50 μg ml^{-1} hygromycin. Cultures were scale-up in glass sterile bottles under shaking until reaching a final volume of 3.0 L cell culture in exponential phase (1–1.5 × 10^7 cells ml^{-1}). *T. cruzi* epimastigotes (Y strain) were grown at 28°C in LIT medium (Bone and Steinert, 1956) supplemented with 10% heat-inactivated FBS. Cultures were scale-up in glass sterile bottles under shaking until reaching a final volume of approximately 1.0 L cell culture in exponential phase (~4 × 10^7 cells ml^{-1}). *T. cruzi* trypomastigotes and amastigotes (Y strain) were collected from the culture medium of infected Vero cells, using a modification of the method of Schmatz and Murray as described before (Moreno *et al.*, 1994). Vero cells were grown in RPMI supplemented with 10% FBS and maintained at 37°C with 5% CO$_2$.

Cell lysis for proteomic studies

Approximately 4 × 10^{10} cells (*T. brucei* PCF and *T. cruzi* epimastigotes) were harvested separately by centrifugation at 1,000 × *g* for 15 min at room temperature (RT) and then washed twice with buffer A with glucose (BAG: 116 mM NaCl, 5.4 mM KCl, 0.8 mM MgSO$_4$, 50 mM Hepes, pH 7.2 and 5.5 mM glucose). Cells were resuspended in 5 ml hypotonic lysis buffer plus protease inhibitors (50 mM Hepes, pH 7.0, protease inhibitor cocktail (P8340, 1:250 dilution), 1 mM PMSF, 2.5 mM TPCK and 100 μM E64) and then incubated for 1 h on ice. Three rounds of freeze-thaw were applied to the cells (5 min on dry ice/ethanol bath, 5 min at 37°C in water bath). Then cells were sonicated three times for 30 s at 40% amplitude, keeping them on ice for at least 1 min between pulses. Cell lysis was verified under light microscope and lysates were filtered through a 5 μm pore nitrocellulose membrane to remove cell ghosts. Protein concentration was determined by BCA Protein Assay kit. Cell lysates were stored at −80°C until processed for polyP-binding protein pull down within a week after lysis.

PolyP biotinylation

Biotinylated polyP was prepared as previously described (Choi *et al.*, 2010). Briefly, medium-size polyP (< 1000 mers) was end-labeled by the covalent linkage of a primary biotinylated amine (amine-PEG$_2$-biotin) to the terminal phosphates of polyP in the presence of 1-ethyl-3-[3-dimetyhlamino-propyl]carbodiimide (EDAC) (Choi *et al.*, 2010).

PolyP-binding protein pull down

Twenty mg streptavidin-coated magnetic beads (Dynabeads MyOne Streptavidin T1) were washed three times with dynabeads wash buffer (1 M LiCl, 50 mM Tris-HCl, pH 7.4) in a 15 ml tube using a DynaMag™ magnet. Beads were incubated with 1×10^{-5} moles biotinylated polyP (resuspended in 5 ml dynabeads wash buffer) for 1 h, at RT under rotation. Then, beads were washed twice with 10 ml wash buffer and once with 10 ml 50 mM Tris-HCl, pH 7.4. Ten pull down rounds were performed as follows: 10 mg protein from *T. cruzi* (or *T. brucei*) total lysate were diluted in 10 ml wash buffer (50 mM Tris-HCl pH 7.4, 5 mM EDTA, 0.1% polyethylenglycol (PEG), 0.01% sodium azide) plus phosphatase inhibitors (2 mM imidazole, 1 mM sodium fluoride, 1.15 mM sodium molybdate, 1 mM sodium orthovanadate and 4 mM sodium tartrate) and filtered through a 0.22 μm pore nitrocellulose membrane. Diluted/filtered protein extracts were incubated with 10 mg polyP-coated beads on a rotator for 30 min at RT. Beads were washed five times with 10 ml wash buffer and polyP-binding proteins were eluted with 500 μl elution buffer (1 M NaCl, 50 mM Tris-HCl, pH 7.4). Eluates from 100 mg initial protein extract were combined and precipitated with trichloroacetic acid (TCA). Finally, polyP-binding proteins were resuspended in 500 μl 50 mM Tris-HCl pH 7.4 and quantified by BCA Protein Assay kit. As a control of binding specificity, biotinylated heparin was bound to streptavidin-coated magnetic beads following the same protocol, and then used for protein pull down from *T. cruzi* and *T. brucei* total protein extracts, as performed with polyP-coated beads.

Sample preparation

Samples containing *T. brucei* and *T. cruzi* polyP-binding proteins from two independent experiments were processed at the Protein Sciences Facility of University of Illinois (Urbana, IL) for liquid chromatography tandem mass spectrometry analysis (LC-MS/MS). Sample cleanup was performed using Perfect Focus according to manufacturer's instructions. Protein samples were reduced in 10 mM DTT at 56°C for 30 min and alkylation was performed using 20 mM iodoacetamide for 30 min in the dark. Samples were digested with trypsin (G-Biosciences, St. Louis, MO) at a ratio of 1:10 – 1:50 using a CEM Discover Microwave Digestor (Mathews, SC) at 55°C for 15 min. Digested peptides were extracted with 50% acetonitrile, 5% formic acid, dried under vacuum and resuspended in 5% acetonitrile, 0.1% formic acid for LC-MS/MS analysis.

Mass spectrometry

LC-MS/MS was performed using a Thermo Dionex Ultimate RSLC3000 operating in nano mode at 300 microliters/min with a gradient from 0.1% formic acid to 60% acetonitrile plus 0.1% formic acid in 120 min. The trap column used was a Thermo Acclaim PepMap 100 (100 μm × 2 cm) and the analytical column was a Thermo Acclaim PepMap RSLC (75 μm × 15 cm).

Data analysis

Xcalibur raw files were converted by Mascot Distiller interface (Matrix Science) into peak lists that were submitted to Mascot Server to search against specific protein databases: *T. brucei* Lister 427 and *T. cruzi* CL Brener (Esmeraldo and Non-Esmeraldo-like) on TriTrypDB (Aslett *et al.*, 2010). Proteins found in control samples from *T. cruzi* and *T. brucei* pull downs using heparin-coated beads, with Mascot scores higher than 50, were considered unspecific binding proteins and subtracted from polyP-binding proteomes of *T. cruzi* and *T. brucei* respectively.

PPBD conjugation to Alexa Fluor 488

E. coli TOP10 F' harboring pTrc-PPBD plasmid (Saito *et al.*, 2005) was grown in 550 ml of Luria-Bertani (LB) broth with 50 μg ml^{-1} ampicillin at 37°C until reaching an OD$_{600}$ of 0.6. The recombinant PPBD expression was induced with 1 mM isopropyl β-D-1-thiogalactopyranoside (IPTG) at 37°C for 3 h. Cells were harvested by centrifugation at 10,000 × *g* for 10 min at 4°C and resuspended in 30 ml of binding buffer (phosphate-buffered saline (PBS: 20 mM Na$_2$HPO$_4$, 300 mM NaCl), pH 7.4, plus 10 mM imidazole), containing protease inhibitor cocktail (P8849, 50 μl g^{-1} of pellet), 100 μg ml^{-1} lysozyme, and 75 U benzonase. The sample was incubated on ice for 30 min and then cells were lysed on ice for 2.5 min with 10 s-pulses (20 s between pulses) of a Branson Sonifier Cell Disruptor with Microtip. Cell debris were removed by centrifugation at 20,000 × *g* for 20 min at 4°C. The supernatant was filtered through a 0.45-μm membrane filter and loaded. PPBD purification was performed at 4°C using 1 ml HisPur Ni-NTA Chromatography Cartridge coupled to an ÄKTA Prime Plus chromatography system (GE Healthcare) selecting the standard program His Tag Purification His Trap. The column was washed with binding buffer and PPBD was eluted with elution buffer (PBS, pH 7.4, plus 300 mM imidazole). Both buffers were previously filtered through 0.22-μm membrane filter. The purity of PPBD in the FPLC fractions was determined by SDS-PAGE and the gel was stained with Coomassie Blue G-250. The purest PPBD fractions were combined and the buffer was exchanged to PBS, pH 7.4, using a 3–12 ml 10 kDa Slide-A-Lyzer Dialysis Cassette at 4°C (a total of four buffer exchanges, including an overnight exchange). After dialysis, the sample was concentrated using an Amicon Ultra-15 10K device (Millipore) until reaching a volume of 1–1.5 ml. Protein concentration was quantified by using the BCA Protein Assay kit. Fluorescent labeling of PPBD (100 μg) was done using the Alexa Fluor 488 Microscale Protein

Labeling kit as recommended by the manufacturer. Alexa Fluor 488-labeled PPBD was kept in 10% glycerol at –20ºC and protected from light for further experiments. Alexa Fluor 488-labeled PPBD concentration (in mg ml^{-1}) was determined by absorbance at 280 nm (A_{280}) and at 494 nm (A_{494}) according to the manufacturer's manual.

Localization of polyP and co-localization with cellular markers in *T. brucei* and *T. cruzi*

Alexa Fluor 488-labeled PPBD was used for localization of polyP and co-localization with cellular markers in PCF and BSF of *T. brucei,* and in epimastigotes, trypomastigotes and amastigotes of *T. cruzi*. Incubations with PPBD were always performed in tris-buffered saline (TBS: 100 mM Tris-HCl, 150 mM NaCl).

For co-localization of PPBD and mitochondria, PCF and BSF live cells were labeled for 30 min with 50 nM MitoTracker Red CMXRos in the corresponding culture medium before the immunofluorescence assays.

PCF (Lister 427), and Y strain epimastigotes and trypomastigotes/amastigotes were washed twice with BAG and then fixed with 4% paraformaldehyde in TBS, pH 7.4 (TBS1) at RT for 1 h. BSF (Lister 427) were washed with ice-cold TBS1 containing 1% glucose and then fixed with 1% paraformaldehyde in the same buffer at 4°C for 1 h. After fixation, all cells were washed twice with TBS1 and allowed to adhere to poly-L-lysine-coated coverslips for 30 min. The coverslips were washed three times with TBS1 and the fixed parasites were permeabilized with 0.3% Triton X-100 in TBS1 for 3 min for PCF, epimastigotes, and trypomastigotes/amastigotes or 0.1% Triton X-100 in TBS1 for 3 min for BSF. Coverslips were washed twice with TBS1 and blocked with TBS1 containing 5% goat serum, 50 mM NH$_4$Cl, 3% BSA, 1% fish gelatin at 4°C overnight.

After blocking, for co-localization with mitochondria, cells which were pre-incubated with MitoTracker were then incubated with Alexa Fluor 488-labeled PPBD (8 µg ml^{-1}) diluted in 1% BSA in TBS, pH 8.0 (TBS2), for 1 h, at RT in the dark.

For co-localization with other cellular compartments, after blocking cells were concomitantly incubated with Alexa Fluor 488-labeled PPBD (8 µg ml^{-1}) and one of the following primary antibodies diluted in 1% BSA in TBS2 for 1 h at RT in the dark: monoclonal mouse anti-TbPPDK antibody (glycosomal marker, 1:30 dilution), polyclonal rabbit anti-TbVP1 antibody (acidocalcisomal marker, 1:500 dilution for PCF, 1:1,000 dilution for BSF, epimastigotes, and trypomastigotes/amastigotes), or polyclonal rabbit anti-BiP antibody (endoplasmic reticulum marker, 1:500). All these coverslips were washed three times with 1% BSA in TBS2 and then incubated with Alexa Fluor 546-conjugated goat anti-rabbit or Alexa Fluor 546-conjugated goat anti-mouse secondary antibodies (1:1,000 dilution) diluted in 1% BSA in TBS2 for 1 h at RT in the dark.

For the co-localization of PPBD and a nucleolus marker in PCF, following the blocking step, an immunofluorescence assay with three incubation steps was performed due to PPBD works well in TBS but not in PBS, and L1C6 antibody works well in PBS: (i) incubation with monoclonal mouse L1C6 antibody (1:200 dilution in PBS, pH 8.0, plus 1% BSA) followed by three washes with the same buffer; (ii) incubation

with the secondary antibody Alexa Fluor 546-conjugated goat anti-mouse (1:1,000 dilution in 1% BSA in PBS, pH 8.0) in the dark followed by three washes with TBS2 and (iii) incubation with Alexa Fluor 488-labeled PPBD (2 µg ml^{-1} in TBS2 plus 1% BSA) in the dark; all incubations for 1 h at RT. In this case, PPBD was used at a lower concentration to minimize glycosomal labeling and show mainly the nucleolus labeling.

For all IFAs cited above, following the final incubation step with either PPBD or antibody, cells were washed three times with 1% BSA in TBS2, washed once with TBS2 and counterstained with DAPI (3 µg ml^{-1}) in Fluoromount-G mounting medium on the slides. Differential interference contrast and fluorescent optical images were taken with a 100X oil immersion objective (1.35 aperture) under non-saturating conditions with a Photometrix CoolSnapHQ charge-coupled device camera driven by DeltaVision software (Applied Precision, Issaquah, WA) and deconvolved for 15 cycles using SoftWoRx deconvolution software. For super-resolution microscopy images were taken with a 100X oil immersion objective, a high-power solid-state 405 nm laser and EM-CCD camera (Andor iXon) under non-saturating conditions in a Zeiss ELYRA S1 (SR-SIM) super-resolution microscope. Images were acquired and processed with ZEN 2011 software with SIM analysis module. Videos were done with Imaris Version 8.0 software using the Surface Reconstruction and Animation functions. For conventional fluorescent images of *T. cruzi* epimastigotes showing cytosolic and nucleolar PPBD labeling, images were acquired using a 100X oil immersion objective, with an Olympus BX60 fluorescence microscope coupled to Olympus DP70 digital camera, and processed with DP controller software.

Effect of polyP in PPBD labeling

T. brucei PCF Lister 427 parasites were washed twice with BAG and fixed with 4% paraformaldehyde in TBS1 for 1 h at RT. After fixation, cells were washed twice with the same buffer and allowed to adhere to poly-L-lysine-coated coverslips for 30 min. The coverslips were washed three times with TBS1 and incubated with 0.3% Triton X-100 in TBS1 for 3 min. Permeabilized cells were washed twice with TBS1 and blocked with the same buffer, containing 5% goat serum, 50 mM NH$_4$Cl, 3% BSA, and 1% fish gelatin at 4°C overnight. In separate tubes, Alexa Fluor 488-labeled PPBD (8 µg ml^{-1}) was pre-incubated in the absence or the presence of polyP diluted in TBS2 containing 1% BSA at RT for 1 h in the dark. Three independent experiments of two types of assays were done: (i) varying the concentration of polyP$_{100}$: 1, 10, 100, and 1000 µM (in phosphate units) and (ii) varying the polyP chain length: 1 mM polyP (in phosphate units) of polyP$_3$, polyP$_{60}$, polyP$_{100}$ and polyP$_{700}$. These samples were then incubated with the parasites-coated coverslips for 1 h at RT in the dark. In both cases, a control was done by incubation of the coverslips with Alexa Fluor 488-labeled PPBD that was not pre-incubated with polyP. The cells were washed three times with 1% BSA in TBS2, washed once with TBS2, and counterstained with DAPI (3 µg ml^{-1}) in Fluoromount-G mounting medium on the slides. Differential interference contrast and fluorescent optical images were taken as above. Cells were imaged and fluorescence intensity of

each cell was quantified after subtracting background fluorescence, using an image processing software (FiJi, Image J, University of Wisconsin-Madison, WI). The averages of fluorescence intensities were calculated and the relative fluorescence (in comparison to the control, using PPBD that was not pre-incubated with polyP) was plotted using GraphPad Prism software. For the assay with variation of polyP$_{100}$ concentration, we examined fluorescence intensity of at least 42 cells from at least 10 fields per replicate, totalizing 471 cells for three biological replicates. For the assay with different polyP chain lengths, at least 56 cells from at least 20 fields per replicate, totalizing 664 cells for three biological replicates.

Subcellular fractionation

Fractions enriched in glycosomes were isolated and purified using two iodixanol gradient centrifugations as described previously (Huang *et al.*, 2014), with some modifications (Fig. S6). PCF trypanosomes (3–4 g wet weight) were washed twice with Buffer A with glucose (BAG), and once with cold isolation buffer (125 mM sucrose, 50 mM KCl, 4 mM MgCl$_2$, 0.5 mM EDTA, 20 mM Hepes, 5 mM dithiothreitol (DTT)) supplied with Complete, EDTA-free, protease inhibitor cocktail (Roche) prior to lysis with silicon carbide in isolation buffer. Silicon carbide and cell debris were eliminated by a series of low-speed centrifugations (100 × *g* for 5 min, 300 × *g* for 10 min, and 1,200 × *g* for 10 min). The supernatant was centrifuged at 17,000 × *g* for 10 min, and the pellet was resuspended in 2.2 ml isolation buffer and applied to the 20% step of a discontinuous gradient with 4 ml steps of 20, 24, 28, 34, 37 and 40% iodixanol (diluted in isolation buffer). The gradient was centrifuged at 50,000 *g* in a Beckman JS-24.38 rotor for 60 min at 4°C, and fractions were collected from the top. The fractions containing crude glycosomes or acidocalcisomes (Fig. S6) were combined and then washed twice with 25 ml isolation buffer by centrifugation at 17,000 *g* for 15 min at 4°C. The washed pellet containing acidocalcisomes was used for polyP extraction and analysis. The washed pellet containing crude glycosomes was resuspended in 700 µl isolation buffer and applied to the 27% step of another discontinuous gradient of iodixanol, with 1.4 ml of isolation buffer containing 10% w/v sucrose over-layered on the top and 1 ml steps of 27, 62 and 80% iodixanol, which were diluted from 90% w/v iodixanol with isolation buffer. To prepare 90% w/v iodixanol, 60% w/v iodixanol solution (Optiprep) was dried completely at 70°C and resuspended with isolation buffer. After the second gradient centrifugation at 50,000 *g* for 60 min at 4°C, fractions were collected from the top, washed twice with isolation buffer by centrifugation at 20,000 *g* for 15 min at 4°C, and analyzed by glycosome or acidocalcisome marker enzyme assays. The protein concentration was quantified by Bradford assay using a SpectraMax Microplate Reader. The fractions 1 and 2, containing approximately 70% (Fig. 5A) of total proteins with the highest hexokinase activity (Fig. 5B), were combined and used for polyP extraction and analyses. Hexokinase (glycosome marker) and pyrophosphatase (PPase) (acidocalcisome marker) activities and immuno-blots were assayed as described previously (Huang *et al.*, 2014). Mouse antibodies against TbPPDK

(1:200) or rabbit antibodies against TbVP1 (1:3,000) were used as indicated.

Molecular constructs and transfection

For the amplification of *ScPPX1* (*S. cerevisiae* PPX) gene (GeneBank ID L28711.1) by PCR, the following primers were designed: ScPPX1-F (5′-TACCCAACTC**GCTAGC**TCGCCTTTGAGAAAGACGGTTCCTG-3′), and ScPPX1-R (5′-CCTTGCTCAC**GCTAGC**CTCTTCCAGGTTT GAGTACGCTTCC-3′), (*Nhe*I restriction sites are in bold), and pTrcHisB-ScPPX1 plasmid (Wurst *et al.*, 1995) was used as DNA template. PCR analysis was done in a reaction volume of 100 µl using Phusion High-Fidelity DNA polymerase with 20 ng of DNA, as follows: initial denaturation for 30 s at 98°C, followed by 30 cycles of 10 s at 98°C, 30 s at 55°C, 1 min at 72°C and then a final extension for 10 min at 72°C. The pXS2-AldoPTS2-eYFP vector (Bauer *et al.*, 2013), which provides resistance to blasticidin, was digested with *Nhe*I-HF. The 1.2 Kb-insert *ScPPX1* was then cloned into *Nhe*I-digested pXS2-AldoPTS2-eYFP vector using the In-Fusion HD Cloning kit, generating the *pXS2-PTS2-ScPPX1-eYFP* plasmid. The recombination product was transformed into *E. coli* Stellar Competent Cells following the manufacturer's instructions. The recombinant construct was confirmed by digestion with restriction enzymes, and sequencing. For *T. brucei* transfection, *pXS2-PTS2-ScP-PX1-eYFP* plasmid was linearized with *Mlu*I and purified with QIAGEN's DNA purification kit.

To attempt to deliver EcPPX (L06129.1) to the nucleolus of *T. brucei*, we designed the primers NoLS-EcPPX-F (5′-CCC**AAGCTT**AAACCACC ATG<u>CGTATCGGAGGGAGACGGAAGGCTAACCCTC ACCTTTTGCGTGAGATAGCTGATGTGACGATG GAGTTGAAAAGATATAGGAAGGGTCGTA GTGGT</u>CCAATACACGATAAATCCCCTCGTC-3′) and EcPPX-R (5′-GC**TCTAGA**AGCGGCGATTTCTGGTG TACTTTCTTC-3′);respective *Hind*III and *Xba*I restriction sites are in bold and a reported NoLS sequence is underlined (Hoek *et al.*, 2000). NLS-EcPPX-HA plasmid was used as DNA template. PCR analysis was done in a reaction volume of 100 µl using Phusion High-Fidelity DNA polymerase with 20 ng of DNA, as follows: initial denaturation for 30 s at 98°C, followed by 30 cycles of 10 s at 98°C, 30 s at 55°C, 1 min at 72°C and then a final extension for 10 min at 72°C. The 1.6 Kb-insert *NoLS-EcPPX* and the vector pLEW100-MCS-GFP were digested with *Hind*III-HF and *Xba*I. The ligation of *NoLS-EcPPX* and pLEW100-MCS-GFP was done with LigaFast Rapid DNA Ligation System, originating NoLS-EcPPX-GFP plasmid. The recombination product was transformed into Zymo 5α Mix & Go competent cells according to manufacturer's instructions. The recombinant constructs were confirmed by digestion with restriction enzymes, and sequencing. For *T. brucei* transfection, NoLS-EcPPX-GFP plasmid was linearized with *Not*I-HF and purified with QIAGEN's DNA purification kit.

T. brucei PCF Lister 427 was used for transfection of the *PTS2-ScPPX1-eYFP* plasmid. *T. brucei* PCF 29-13 was used for transfection of the plasmid NoLS-EcPPX-GFP. Cell transfections were done as reported previously (Huang *et al.*, 2014). In brief, parasites in exponential phase were harvested by centrifugation at 1,000 × *g* for 7 min at RT, washed

once with 10 ml of Cytomix buffer (2 mM EGTA, 5 mM MgCl$_2$, 120 mM KCl, 0.15 mM CaCl$_2$, 10 mM K$_2$HPO$_4$, 25 mM Hepes, 0.5 % glucose, 0.1 mg ml^{-1} bovine serum albumin and 1 mM hypoxanthine, pH 7.6) and resuspended in 0.45 ml of the same buffer at a cell density of 1.5 × 10^8 cells ml^{-1} (7 × 10^7 cells per cuvette). The washed cells were mixed with 10 µg of plasmid in a 4 mm electroporation cuvette and subjected to two pulses from a Bio-Rad Gene Pulser Xcell electroporator set at 1,500 V, 25 µF, 200 Ω, with resting on ice for 1 min between pulses. Negative controls were flasks containing cells without plasmid DNA, submitted to the electroporation and flasks containing cells without plasmid DNA that were not submitted to electroporation. Transfectant PTS2-ScPPX1-eYFP was cultured in SDM-79 medium supplemented with 15% heat-inactivated FBS plus 10 µg ml^{-1} blasticidin until stable cell lines were obtained. The protein PTS2-ScPPX1-eYFP is constitutively expressed in these parasites. Transfectant *NoLS-EcPPX-GFP*-expressing cells were cultured in SDM-79 medium supplemented with 15% tetracycline-free and heat-inactivated FBS plus 50 µg ml^{-1} hygromycin, 15 µg ml^{-1} G418 and 10 µg ml^{-1} blasticidin until stable cell lines were obtained.

Western blot analyses

To confirm the expression of the protein PTS2-ScPPX1-eYFP, mid log phase parasites from PCF wild type and *PTS2-ScPPX1-eYFP*-expressing cells were harvested by centrifugation at 1,000 × *g* for 7 min and washed twice with BAG at RT. The pellet was resuspended in 200 µl of RIPA buffer (150 mM NaCl, 20 mM Tris-HCl, pH 7.5, 1 mM EDTA, 1% sodium dodecyl sulphate and 0.1% Triton X-100) plus 2 mM phenylmethanesulfonyl fluoride (PMSF), and protease inhibitor cocktail (P8340, 1:250 dilution). The samples were incubated on ice for 1 h and then homogenized with a 1 ml syringe. The lysates were kept at −80°C until further use. The protein concentration in the lysates was determined using the BCA Protein Assay Kit. Approximately 20 µg of each lysate were submitted to electrophoresis using 4–20% Mini-Protean TGX Precast Protein Gel. Magic Mark XP Western Protein Standard was applied on the gel. Electrophoresed proteins were transferred to nitrocellulose membranes using a Bio-Rad transblot apparatus for 1 h at 100 V at 4°C. Following transfer, the membrane blots were blocked with 5% non-fat dry milk in PBS containing 0.1% (v/v) Tween-20 (PBS-T) at 4°C overnight. Blots were probed with polyclonal rabbit anti-GFP antibody (1:10,000 dilution in PBS-T) or polyclonal rabbit anti-tubulin antibody (1:20,000 dilution in PBS-T) for 1 h at RT. After washing three times with PBS-T, the blots were incubated with horseradish peroxidase conjugated anti-rabbit IgG antibody (1:20,000 dilution in PBS-T) for 1 h at RT. The membranes were washed three times with PBS-T, and western blot images were processed and analyzed using ECL Western Blotting Substrate according to the manufacturer's instructions.

For expression of the protein NoLS-EcPPX-GFP, the culture was induced with 1 µg ml^{-1} tetracycline for 48 h. Lysates from non-induced and induced cultures were analysed by western blot that were performed as above with the following modifications. Approximately 50 µg of each lysate were submitted to electrophoresis using 10% SDS-PAGE. Blots were probed with polyclonal rabbit anti-GFP antibody (1:10,000 dilution in PBS-T) or polyclonal rabbit anti-tubulin antibody (1:20,000 dilution in PBS-T) for 1 h at RT.

For loading control of Fig. 6D, the western blot was performed using rabbit anti-tubulin antibody (1:10,000 dilution) and IRDye 680RD goat anti-rabbit (1:20,000 dilution) and was analyzed with Li-Cor Odyssey CLx Imaging System.

Immunofluorescence analyses

For immunofluorescence assays of PCF expressing PTS2-ScPPX1-eYFP, the cells were washed twice with BAG and fixed with 4% paraformaldehyde in PBS, pH 7.4, (PBS1) for 1 h at RT. After fixation, cells were washed twice with the same buffer and allowed to adhere to poly-L-lysine-coated coverslips for 30 min. The coverslips were washed three times with PBS1 and incubated with 0.3% Triton X-100 in PBS1 for 3 min. Permeabilized cells were washed twice with PBS1 and blocked with PBS1 containing 5% goat serum, 50 mM NH$_4$Cl, 3% BSA, and 1% fish gelatin, at 4°C overnight. After blocking, cells were incubated with the primary antibodies, polyclonal rabbit anti-GFP antibody (1:1,000 dilution) and monoclonal mouse anti-PPDK antibody (1:30 dilution) diluted in 1% BSA in PBS, pH 8.0 (PBS2) for 1 h at RT. The coverslips were washed three times with 1% BSA in PBS2 and then incubated with Alexa Fluor 488-conjugated goat anti-rabbit and Alexa Fluor 546-conjugated goat anti-mouse secondary antibodies (1:1,000 dilution) diluted in 1% BSA in PBS2 for 1 h at RT in the dark. The cells were washed three times with 1% BSA in PBS2, washed once with PBS2 and counterstained with DAPI (3 µg ml^{-1}) in Fluoromount-G mounting medium on the slides. Two negative controls were done, wild type PCF Lister 427, according to the protocol described above, and PTS2-ScPPX1-transfected PCF in the absence of primary antibodies. Differential interference contrast and fluorescent optical images were taken with DeltaVision system as described above. Pearson's correlation coefficient was calculated using the SoftWoRx software by measuring the whole-cell images.

NoLS-EcPPX-GFP culture was induced with 1 µg ml^{-1} tetracycline for 24 h and IFA was performed as above with some modifications related to antibody incubations. A two-step IFA was chosen for *NoLS-EcPPX-GFP*-expressing cells due to PPBD works well in TBS but not in PBS, and rabbit anti-GFP antibody works well in PBS: until incubation with primary antibodies, PBS1 was used. Cells were then incubated with polyclonal rabbit anti-GFP antibody (1:2,000 dilution) diluted in 1% BSA in PBS2. Afterwards cells were washed three times with TBS2 and then concomitantly incubated with the secondary antibody Alexa Fluor 546-conjugated goat anti-rabbit, and PPBD (8 µg ml^{-1}), diluted in 1% BSA in TBS2. From this step all washes were done in TBS2. The negative control consisted in non-induced cells.

PPX activity determination

Parasites (4.5 × 10^7 cells) from wild type (Lister 427) and *PTS2-ScPPX1*-expressing PCF were harvested by centrifugation at 1,000 × *g* for 7 min at RT, washed twice with BAG at RT, and resuspended in 1 ml of resuspension buffer (150 mM NaCl, 20 mM Tris-HCl pH 7.5, 1 mM EDTA,

2 mM PMSF, and protease inhibitor cocktail (1:250 dilution, P8340)). Cells were lysed by 7 cycles of freezing and thawing (for freezing steps, the tubes were incubated in dry ice/ethanol bath, and for thawing steps, in water at RT) and then the lysates were homogenized using a 1 ml-syringe. In a 96-well plate, 20 μl of each lysate were incubated in the presence or the absence of 10 μM polyP$_{100}$ (in phosphate units) in activity buffer (50 mM Tris-HCl pH 7.4, and 2.5 mM MgSO$_4$) at 30°C for 10 min, totalizing 100 μl of reaction volume. Negative controls were reaction buffers without lysates (blank) and lysates kept on ice (sample named 'ice' on the graph). After the incubation time, the reactions were stopped by the addition of 100 μl of freshly prepared malachite green solution (three parts of 0.045% malachite green and one part of 4.2% ammonium molybdate/4 M HCl) (Lanzetta *et al.*, 1979). Release of phosphate from polyP due to the PPX activity was measured in triplicate wells by reading the absorbance at 660 nm immediately on the plate reader Biotek Synergy H1. Three independent experiments were done. In all biological replicates, a standard curve of potassium phosphate was included in triplicate wells.

Short- and long-chain polyP extraction and analysis

Short-chain polyP was extracted from wild type (Lister 427) and *PTS2-ScPPX1*-expressing PCF using a protocol reported previously (Ruiz *et al.*, 2001). Long-chain polyP was extracted from cells or from subcellular fractions according to a published protocol (Ault-Riche *et al.*, 1998).

Quantification of short- and long-chain polyP (both extracted from 10^8 cells) was determined by measuring the amount of P_i released upon addition of recombinant ScPPX1 to the plate wells. For both short- and long-chain polyP quantification, 10 μl of polyP were incubated with 90 ng of recombinant ScPPX1 in activity buffer (50 mM Tris-HCl pH 7.4, and 2.5 mM MgSO$_4$) at 30°C for 1 h, in a final volume of 100 μl. A negative control was reaction buffer without enzyme. The rest of the protocol was followed as cited in the previous section. Three independent experiments were performed.

Short-chain polyP was also resolved by PAGE. PCF (2 × 10^9 cells) were harvested by centrifugation at 1,000 × *g* for 7 min and washed twice with BAG. For loading controls, we collected from each sample 10^8 cells that were immediately lysed with RIPA buffer, the protein concentration measured using BCA Protein Assay kit (see methods for Western blot analysis) and used for western blot analysis with rabbit anti-tubulin antibodies. The other part of the cell cultures (1.9 × 10^9 cells) was centrifuged at 1,000 × *g* for 7 min and resuspended in 100 μl of ice-cold 1 M perchloric acid (HClO$_4$) for polyP analysis. The samples were incubated on ice for 5 min and cell debris were removed by centrifugation at 18,000 × *g* for 5 min at 4°C. The supernatants were transferred to new tubes and neutralized with 20 μl of neutralizing solution (0.6 M KHCO$_3$, 0.72 M KOH). The pH was checked with pH strips and neutralized to 7.0–7.5, if necessary. The precipitated salt was removed by centrifugation at 18,000 × *g* for 5 min at 4°C. An additional centrifugation step was carried out to eliminate remaining precipitates. The supernatants were immediately submitted to electrophoresis or kept at –80°C until further use. Short-chain polyP was resolved by PAGE using 35.5% acrylamide/bis-acrylamide 19:1 gels

in Tris/Borate/EDTA (TBE) buffer. Gels were stained with toluidine blue. PolyP density in each gel lane was quantified using FiJi software. Four independent experiments were done.

Analysis of long-chain polyP in subcellular fractions from wild type PCF was done by PAGE using a 30% acrylamide/bis-acrylamide 19:1 gel stained with toluidine blue. Three independent biological experiments were done.

Effect of oxidative stress

Wild type (Lister 427) and *PTS2-ScPPX1*-expressing PCF (1.2 × 10^8 cells) were harvested by centrifugation at 1,000 × *g* for 7 min and resuspended in 4 ml of SDM-79 medium plus 10% heat-inactivated FBS (with the addition of 10 μg ml^{-1} blasticidin to *PTS2-ScPPX1*-expressing PCF). Hydrogen peroxide (H$_2$O$_2$, 50 μM) was added and the cells were incubated at 28°C for 1 h. Cultures were then diluted 10 times (with addition of blasticidin to the medium of *PTS2-ScPPX1*-expressing PCF) and incubated at 28°C for 24 h. The cell density after 24 h was determined by counting parasites in a Neubauer chamber. Three independent experiments were done.

Glucose consumption

Wild type (Lister 427) and *PTS2-ScPPX1*-expressing PCF (10^8 cells ml^{-1}) were incubated in a modified SDM-79 medium (without phenol red and hemin plus 10% heat-inactivated FBS and addition of 10 μg ml^{-1} blasticidin to the *PTS2-ScPPX1*-expressing cells) for 6 h at 28°C. 100 μl of both cultures at time 0 and after 6 h of incubation were centrifuged at 14,000 × *g* for 1 min. Two microliters of each supernatant were used to quantify glucose in triplicate plate wells, using the D-Glucose Assay Kit. After addition of 200 μl of glucose oxidase/peroxidase (GOPOD) reagent to each well, the plate was incubated at 48°C for 20 min. The absorbance was read at 510 nm on the Biotek Synergy H1 plate reader. Three independent experiments were done. In all biological replicates, a standard curve of glucose was included in triplicate wells. The glucose consumption plotted in the graph was calculated by the difference in the amount of glucose in the supernatants at time 0 and after 6 h of incubation.

Statistical analyses

Values are expressed as means ± SEM, or means ± SD, as indicated. Significant differences between treatments were compared using unpaired Student's *t*-test, and one-way and two-way ANOVA tests. Differences were considered statistically significant at *P* < 0.05, and *n* refers to the number of experiments performed. All statistical analyses were conducted using GraphPad Prism 6 (GraphPad Software, San Diego, CA).

Author contributions

R.S.N., N.L., G.H., C.D.C. and R.D. designed the experiments and analyzed the data. R.S.N., N.L., G.H, C.D.C. and S.S. conducted the experiments. R.D. wrote the majority of the manuscript, with specific sections contributed by R.S.N., N.L., C.D.C., S.S. and J.H.M. R.D., G.H. and J.H.M supervised the work and contributed to the analysis of experiments.

References

Acosta, H., Dubourdieu, M., Quinones, W., Caceres, A., Bringaud, F. and Concepcion, J.L. (2004) Pyruvate phosphate dikinase and pyrophosphate metabolism in the glycosome of *Trypanosoma cruzi* epimastigotes. *Comparative Biochemistry and Physiology Part B: Biochemistry and Molecular Biology*, **138**, 347–356.

Antonenkov, V.D. and Hiltunen, J.K. (2012) Transfer of metabolites across the peroxisomal membrane. *Biochimica et Biophysica Acta (BBA)*, **1822**, 1374–1386.

Aslett, M., Aurrecoechea, C., Berriman, M., Brestelli, J., Brunk, B.P., Carrington, M. *et al.* (2010) TriTrypDB: a functional genomic resource for the Trypanosomatidae. *Nucleic Acids Research*, **38**, D457–462.

Ault-Riche, D., Fraley, C.D., Tzeng, C.M. and Kornberg, A. (1998) Novel assay reveals multiple pathways regulating stress-induced accumulations of inorganic polyphosphate in *Escherichia coli*. *Journal of Bacteriology*, **180**, 1841–1847.

Azevedo, C., Livermore, T. and Saiardi, A. (2015) Protein polyphosphorylation of lysine residues by inorganic polyphosphate. *Molecular Cell*, **58**, 71–82.

Bangs, J.D., Uyetake, L., Brickman, M.J., Balber, A.E. and Boothroyd, J.C. (1993) Molecular cloning and cellular localization of a BiP homologue in *Trypanosoma brucei*. Divergent ER retention signals in a lower eukaryote. *Journal of Cell Science* **105** (Pt, 4), 1101–1113.

Bauer, S., Morris, J.C. and Morris, M.T. (2013) Environmentally regulated glycosome protein composition in the African trypanosome. *Eukaryotic Cell*, **12**, 1072–1079.

Bentley-DeSousa, A., Holinier, C., Moteshareie, H., Tseng, Y.C., Kajjo, S., Nwosu, C. *et al.* (2018) A screen for candidate targets of lysine polyphosphorylation uncovers a conserved network implicated in ribosome biogenesis. *Cell Reports*, **22**, 3427–3439.

Bone, G.J. and Steinert, M. (1956) Isotopes incorporated in the nucleic acids of *Trypanosoma mega*. *Nature*, **178**, 308–309.

Brangwynne, C.P., Mitchinson, T.J. and adn Hyman, A.A. (2011) Active liquid-like behavior of nucleoli determines their size and shape in Xenopu laevis oocytes. *Proceedings of the National Academy of Sciences of the United States of America*, **108**, 4334–4339.

Bringaud, F., Baltz, D. and Baltz, T. (1998) Functional and molecular characterization of a glycosomal PPi-dependent enzyme in trypanosomatids: pyruvate, phosphate dikinase. *Proceedings of the National Academy of Sciences of the United States of America*, **95**, 7963–7968.

Caceres, A.J., Portillo, R., Acosta, H., Rosales, D., Quinones, W., Avilan, L. *et al.* (2003) Molecular and biochemical characterization of hexokinase from *Trypanosoma cruzi*. *Molecular and Biochemical Parasitology*, **126**, 251–262.

Chambers, J.W., Kearns, M.T., Morris, M.T. and Morris, J.C. (2008) Assembly of heterohexameric trypanosome hexokinases reveals that hexokinase 2 is a regulable enzyme. *Journal of Biological Chemistry*, **283**, 14963–14970.

Choi, S.H., Collins, J.N., Smith, S.A., Davis-Harrison, R.L., Rienstra, C.M. and Morrissey, J.H. (2010) Phosphoramidate end labeling of inorganic polyphosphates: facile manipulation of polyphosphate for investigating and modulating its biological activities. *Biochemistry*, **49**, 9935–9941.

Cremers, C.M., Knoefler, D., Gates, S., Martin, N., Dahl, J.U., Lempart, J. *et al.* (2016) Polyphosphate: a conserved modifier of amyloidogenic processes. *Molecular Cell*, **63**, 768–780.

Cunningham, I. and Honigberg, B.M. (1977) Infectivity re-acquisition by *Trypanosoma brucei brucei* cultivated with tsetse salivary glands. *Science*, **197**, 1279–1282.

Devaux, S., Kelly, S., Lecordier, L., Wickstead, B., Perez-Morga, D., Pays, E. *et al.* (2007) Diversification of function by different isoforms of conventionally shared RNA polymerase subunits. *Molecular Biology of the Cell*, **18**, 1293–1301.

Docampo, R. (2016) The origin and evolution of the acidocalcisome and its interactions with other organelles. *Molecular and Biochemical Parasitology*, **209**, 3–9.

Docampo, R., de Souza, W., Miranda, K., Rohloff, P. and Moreno, S.N. (2005) Acidocalcisomes – conserved from bacteria to man. *Nature Reviews Microbiology*, **3**, 251–261.

Docampo, R. and Huang, G. (2016) Acidocalcisomes of eukaryotes. *Current Opinion in Cell Biology*, **41**, 66–72.

Fang, J., Rohloff, P., Miranda, K. and Docampo, R. (2007a) Ablation of a small transmembrane protein of *Trypanosoma brucei* (TbVTC1) involved in the synthesis of polyphosphate alters acidocalcisome biogenesis and function, and leads to a cytokinesis defect. *Biochemical Journal*, **407**, 161–170.

Fang, J., Ruiz, F.A., Docampo, M., Luo, S., Rodrigues, J.C., Motta, L.S. *et al.* (2007b) Overexpression of a Zn^{2+}-sensitive soluble exopolyphosphatase from *Trypanosoma cruzi* depletes polyphosphate and affects osmoregulation. *The Journal of Biological Chemistry*, **282**, 32501–32510.

Gabaldon, T., Ginger, M.L. and Michels, P.A. (2016) Peroxisomes in parasitic protists. *Molecular and Biochemical Parasitology*, **209**, 35–45.

Gomez-Garcia, M.R., Ruiz-Perez, L.M., Gonzalez-Pacanowska, D. and Serrano, A. (2004) A novel calcium-dependent soluble inorganic pyrophosphatase from the trypanosomatid *Leishmania major*. *FEBS Letters*, **560**, 158–166.

Gray, M.J., Wholey, W.Y., Wagner, N.O., Cremers, C.M., Mueller-Schickert, A., Hock, N.T. *et al.* (2014) Polyphosphate is a primordial chaperone. *Molecular Cell*, **53**, 689–699.

Griffin, J.B., Davidian, N.M. and Penniall, R. (1965) Studies of phosphorus metabolism by isolated nuclei. VII. Identification of polyphosphate as a product. *The Journal of Biological Chemistry*, **240**, 4427–4434.

Gualdron-Lopez, M., Vapola, M.H., Miinalainen, I.J., Hiltunen, J.K., Michels, P.A. and Antonenkov, V.D. (2012) Channel-forming activities in the glycosomal fraction from the bloodstream form of *Trypanosoma brucei*. *PLoS One*, **7**, e34530.

Guther, M.L., Urbaniak, M.D., Tavendale, A., Prescott, A. and Ferguson, M.A. (2014) High-confidence glycosome proteome for procyclic form *Trypanosoma brucei* by epitope-tag organelle enrichment and SILAC proteomics. *Journal of Proteome Research*, **13**, 2796–2806.

Hoek, M., Engstler, M. and Cross, G.A. (2000) Expression-site-associated gene 8 (ESAG8) of *Trypanosoma brucei* is apparently essential and accumulates in the nucleolus. *Journal of Cell Science*, **113**(Pt 22), 3959–3968.

Hothorn, M.N.H., Lenherr E.D., Wehner M., Rybin V., Hassa P.O., Uttenweiler A. *et al.* (2009) Catalytic core of a membrane-associated eukaryotic polyphosphate polymerase. *Science*, **324**, 513–516.

Huang, G., Ulrich, P.N., Storey, M., Johnson, D., Tischer, J., Tovar, J.A. (2014) Proteomic analysis of the acidocalcisome, an organelle conserved from bacteria to human cells. *PLoS Pathogens*, **10**, e1004555.

Jimenez-Nunez, M.D., Moreno-Sanchez, D., Hernandez-Ruiz, L., Benitez-Rondan, A., Ramos-Amaya, A., Rodriguez-Bayona, B. (2012) Myeloma cells contain high levels of inorganic polyphosphate which is associated with nucleolar transcription. *Haematologica*, **97**, 1264–1271.

Kampinga, H.H. (2014) Chaperoned by prebiotic inorganic polyphosphate molecules: an ancient transcription-independent mechanism to restore protein homeostasis. *Molecular Cell*, **53**, 685–687.

Klompmaker, S.H., Kohl, K., Fasel, N. and Mayer, A. (2017) Magnesium uptake by connecting fluid-phase endocytosis to an intracellular inorganic cation filter. *Nature Communications*, **8**, 1879.

Kornberg, A. (1995) Inorganic polyphosphate: toward making a forgotten polymer unforgettable. *Journal of Bacteriology*, **177**, 491–496.

Kulaev, I. and Kulakovskaya, T. (2000) Polyphosphate and phosphate pump. *Annual Review of Microbiology*, **54**, 709–734.

Kumble, K.D. and Kornberg, A. (1995) Inorganic polyphosphate in mammalian cells and tissues. *Journal of Biological Chemistry*, **270**, 5818–5822.

Kuroda, A., Nomura, K., Ohtomo, R., Kato, J., Ikeda, T., Takiguchi, N. *et al.* (2001) Role of inorganic polyphosphate in promoting ribosomal protein degradation by the Lon protease in *E. coli*. *Science*, **293**, 705–708.

Landeira, D. and Navarro, M. (2007) Nuclear repositioning of the VSG promoter during developmental silencing in *Trypanosoma brucei*. *The Journal of Cell Biology*, **176**, 133–139.

Lander, N., Ulrich, P.N. and Docampo, R. (2013) *Trypanosoma brucei* vacuolar transporter chaperone 4 (TbVtc4) is an acidocalcisome polyphosphate kinase required for in vivo infection. *The Journal of Biological Chemistry*, **288**, 34205–34216.

Lanzetta, P.A., Alvarez, L.J., Reinach, P.S. and Candia, O.A. (1979) An improved assay for nanomole amounts of inorganic phosphate. *Analytical Biochemistry*, **100**, 95–97.

Lemercier, G., Dutoya, S., Luo, S., Ruiz, F.A., Rodrigues, C.O., Baltz, T. (2002) A vacuolar-type H^+-pyrophosphatase governs maintenance of functional acidocalcisomes and growth of the insect and mammalian forms of *Trypanosoma brucei*. *The Journal of Biological Chemistry*, **277**, 37369–37376

Lemercier, G., Espiau, B., Ruiz, F.A., Vieira, M., Luo, S., Baltz, T. *et al.* (2004) A pyrophosphatase regulating polyphosphate metabolism in acidocalcisomes is essential for *Trypanosoma brucei* virulence in mice. *The Journal of Biological Chemistry*, **279**, 3420–3425.

Lonetti, A., Szijgyarto, Z., Bosch, D., Loss, O., Azevedo, C. and Saiardi, A. (2011) Identification of an evolutionarily conserved family of inorganic polyphosphate endopolyphosphatases. *The Journal of Biological Chemistry*, **286**, 31966–31974.

Lynn, W.S. and Brown, R.H. (1963) Synthesis of polyphosphate by rat liver mitochondria. *Biochemical and Biophysical Research Communications*, **11**, 367–371.

Maldonado, R.A. and Fairlamb, A.H. (2001) Cloning of a pyruvate phosphate dikinase from *Trypanosoma cruzi*. *Molecular and Biochemical Parasitology*, **112**, 183–191.

Mani, J., Guttinger, A., Schimanski, B., Heller, M., Acosta-Serrano, A., Pescher, P. *et al.* (2011) Alba-domain proteins of *Trypanosoma brucei* are cytoplasmic RNA-binding proteins that interact with the translation machinery. *PLoS One*, **6**, e22463.

McInerney, P., Mizutani, T. and Shiba, T. (2006) Inorganic polyphosphate interacts with ribosomes and promotes translation fidelity *in vitro* and *in vivo*. *Molecular Microbiology*, **60**, 438–447.

McNae, I.W., Martinez-Oyanedel, J., Keillor, J.W., Michels, P.A., Fothergill-Gilmore, L.A. and Walkinshaw, M.D. (2009) The crystal structure of ATP-bound phosphofructokinase from *Trypanosoma brucei* reveals conformational transitions different from those of other phosphofructokinases. *Journal of Molecular Biology*, **385**, 1519–1533.

Michels, P.A., Chevalier, N., Opperdoes, F.R., Rider, M.H. and Rigden, D.J. (1997) The glycosomal ATP-dependent phosphofructokinase of *Trypanosoma brucei* must have evolved from an ancestral pyrophosphate-dependent enzyme. *European Journal of Biochemistry*, **250**, 698–704.

Michels, P.A., Hannaert, V. and Bringaud, F. (2000) Metabolic aspects of glycosomes in trypanosomatidae – new data and views. *Parasitology Today*, **16**, 482–489.

Michels, P.A. and Opperdoes, F.R. (1991) The evolutionary origin of glycosomes. *Parasitology Today*, **7**, 105–109.

Moreno, B., Urbina, J.A., Oldfield, E., Bailey, B.N., Rodrigues, C.O. and Docampo, R. (2000) ^{31}P NMR spectroscopy of *Trypanosoma brucei, Trypanosoma cruzi,* and *Leishmania major*. Evidence for high levels of condensed inorganic phosphates. *The Journal of Biological Chemistry*, **275**, 28356–28362.

Moreno, S.N. and Docampo, R. (2013) Polyphosphate and its diverse functions in host cells and pathogens. *PLoS Pathogens*, **9**, e1003230.

Moreno, S.N., Silva, J., Vercesi, A.E. and Docampo, R. (1994) Cytosolic-free calcium elevation in *Trypanosoma cruzi* is required for cell invasion. *Journal of Experimental Medicine*, **180**, 1535–1540.

Moreno-Sanchez, D., Hernandez-Ruiz, L., Ruiz, F.A. and Docampo, R. (2012) Polyphosphate is a novel pro-inflammatory regulator of mast cells and is located in acidocalcisomes. *The Journal of Biological Chemistry*, **287**, 28435–28444.

Offenbacher, S. and Kline, E.S. (1984) Evidence for polyphosphate in phosphorylated nonhistone nuclear proteins. *Archives of Biochemistry and Biophysics*, **231**, 114–123.

Opperdoes, F.R. and Borst, P. (1977) Localization of nine glycolytic enzymes in a microbody-like organelle in *Trypanosoma brucei:* the glycosome. *FEBS Letters*, **80**, 360–364.

Pabon, M.A., Caceres, A.J., Gualdron, M., Quinones, W., Avilan, L. and Concepcion, J.L. (2007) Purification and characterization of hexokinase from *Leishmania mexicana*. *Parasitology Research*, **100**, 803–810.

Park, J.H., Brekken, D.L., Randall, A.C. and Parsons, M. (2002) Molecular cloning of *Trypanosoma brucei* CK2 catalytic subunits: the alpha isoform is nucleolar and phosphorylates the nucleolar protein Nopp44/46. *Molecular and Biochemical Parasitology*, **119**, 97–106.

Pisoni, R.L. and Lindley, E.R. (1992) Incorporation of [^{32}P] orthophosphate into long chains of inorganic polyphosphate within lysosomes of human fibroblasts. *The Journal of Biological Chemistry*, **267**, 3626–3631.

Ramos, I.B., Miranda, K., Pace, D.A., Verbist, K.C., Lin, F.Y., Zhang, Y. *et al.* (2010) Calcium- and polyphosphate-containing acidic granules of sea urchin eggs are similar to acidocalcisomes, but are not the targets for NAADP. *Biochemical Journal*, **429**, 485–495.

Rao, N.N., Gomez-Garcia, M.R. and Kornberg, A. (2009) Inorganic polyphosphate: essential for growth and survival. *Annual Review of Biochemistry*, **78**, 605–647.

Rodrigues, C.O., Ruiz, F.A., Vieira, M., Hill, J.E. and Docampo, R. (2002) An acidocalcisomal exopolyphosphatase from *Leishmania major* with high affinity for short chain polyphosphate. *The Journal of Biological Chemistry*, **277**, 50899–50906.

Rodriguez, E., Lander, N., and Ramirez, J.L. (2009) Molecular and biochemical characterisation of *Trypanosoma cruzi* phosphofructokinase. *Memórias do Instituto Oswaldo Cruz*, **104**, 745–748.

Ruiz, F.A., Rodrigues, C.O. and Docampo, R. (2001) Rapid changes in polyphosphate content within acidocalcisomes in response to cell growth, differentiation, and environmental stress in *Trypanosoma cruzi*. *The Journal of Biological Chemistry*, **276**, 26114–26121.

Saiardi, A., (2012) How inositol pyrophosphates control cellular phosphate homoeostasis? *Advances in Biological Regulation*, **52**, pp. 351–359.

Saito, K., Kuga-Uetake, Y., Saito, M. and Peterson, R.L. (2006) Vacuolar localization of phosphorus in hyphae of *Phialocephala fortinii,* a dark septate fungal root endophyte. *Canadian Journal of Microbiology*, **52**, 643–650.

Saito, K., Ohtomo, R., Kuga-Uetake, Y., Aono, T. and Saito, M. (2005) Direct labeling of polyphosphate at the ultrastructural level in *Saccharomyces cerevisiae* by using the affinity of the polyphosphate binding domain of *Escherichia coli* exopolyphosphatase. *Applied and Environmental Microbiology*, **71**, 5692–5701.

Scott, D.A., Docampo, R., Dvorak, J.A., Shi, S. and Leapman, R.D. (1997) In situ compositional analysis of acidocalcisomes in *Trypanosoma cruzi*. *The Journal of Biological Chemistry*, **272**, 28020–28029.

Semenyuk, P.I., Muronetz, V.I., Haertle, T. and Izumrudov, V.A. (2013) Effect of poly(phosphate) anions on glyceraldehyde-3-phosphate dehydrogenase structure and thermal aggregation: comparison with influence of poly(sulfoanions). *Biochimica et Biophysica Acta (BBA)*, **1830**, 4800–4805.

Shih, S., Stenberg, P. and Ullman, B. (1998) Immunolocalization of *Trypanosoma brucei* hypoxanthine-guanine phosphoribosyltransferase to the glycosome. *Molecular and Biochemical Parasitology*, **92**, 367–371.

Smith, S.A., Mutch, N.J., Baskar, D., Rohloff, P., Docampo, R. and Morrissey, J.H. (2006) Polyphosphate modulates blood coagulation and fibrinolysis. *Proceedings of the National Academy of Sciences of the United States of America*, **103**, 903–908.

Ulrich, P.N., Lander, N., Kurup, S.P., Reiss, L., Brewer, J., Soares Medeiros, L.C. (2014) The acidocalcisome vacuolar transporter chaperone 4 catalyzes the synthesis of polyphosphate in insect-stages of *Trypanosoma brucei* and *T. cruzi*. *Journal of Eukaryotic Microbiology*, **61**, 155–165.

Vorisek, J., Knotkova, A. and Kotyk, A. (1982) Fine cytochemical localization of polyphosphates in the yeast *Saccharomyces cerevisiae*. *Zentralblatt für Mikrobiologie*, **137**, 421–432.

Wierenga, R.K., Swinkels, B., Michels, P.A., Osinga, K., Misset, O., Van Beeumen, J. *et al.* (1987) Common elements on the surface of glycolytic enzymes from *Trypanosoma brucei* may serve as topogenic signals for import into glycosomes. *The EMBO Journal*, **6**, 215–221.

Wilkinson, S., Meyer, D.J., Taylor, M.C., Bromley, E.V., Miles, M.A. and Kelly, J.M. (2002) The *Trypanosoma cruzi* enzyme TcGPX1 is a glycosomal peroxidase and caan be linked to trypanothione reduction by glutathione or tryparedoxin. *The Journal of Biological Chemistry*, **277**, 17062–17071.

Wurst, H. and Kornberg, A. (1994) A soluble exopolyphosphatase of *Saccharomyces cerevisiae*. Purification and characterization. *The Journal of Biological Chemistry*, **269**, 10996–11001.

Wurst, H., Shiba, T. and Kornberg, A. (1995) The gene for a major exopolyphosphatase of *Saccharomyces cerevisiae*. *Journal of Bacteriology*, **177**, 898–906.

Yang, Y., Ko, T.P., Chen, C.C., Huang, G., Zheng, Y., Liu, W. *et al.* (2016) Structures of trypanosome vacuolar soluble pyrophosphatases: antiparasitic drug targets. *ACS Chemical Biology*, **11**, 1362–1371.

Supporting Information

Additional supporting information may be found online in the Supporting Information section at the end of the article.